

AN ABSTRACT OF THE THESIS OF

Yan Li for the degree of Master of Science in Electrical and Computer Engineering presented on November 20, 2003.

Title: Electromagnetic Analysis of Energy System Devices.

Abstract approved:

Alan K. Wallace

Annette von Jouanne

Many new applications of energy system devices have been developed to save energy, improve the controllability and stability of industrial processes, and reduce the weight, volume and cost of consumer devices. Due to the novelty of these devices, traditional empirical methods and lumped-parameter circuit theory methods are not sufficient for product development and optimization. Electromagnetic analysis approaches can provide accurate parameter calculation and performance prediction for these new products / prototypes of energy system devices. They are powerful and efficient tools for new product development and existing product optimization.

The research analysis work of this thesis applied the LTA (Layer Theory Approach) and FEM (Finite Element Method) to analyze two types of new energy system devices, a permanent magnet coupling and its derivatives and the prototype of a linear reluctance machine, respectively. LTA is a suitable and efficient tool for devices like linear induction machines and permanent magnet couplings, which include sheet conductors as secondaries. FEM is an analysis tool with wider application area. It is applicable for most devices even with complicated structures. But, it has numerous disadvantages including large memory requirements and very long computational times. The performance of a permanent magnet dynamometer-brake coupling was predicted with the LTA program and compared with experimental results. The comparison shows good correlation between the layer model and the test data. The LTA program was also proved to be a useful tool for parametric design studies and conceptual designs for devices such as large quiet

brakes to be used in the testing of drives for Navy ships. 2-D FEM with calibration techniques were adopted to analyze the complicated prototype of a linear reluctance machine. The analysis results successfully helped confirm the operation of the prototype device and investigate its uncompromised performance. In addition, it provides useful information for next generation product development.

©Copyright by Yan Li
November 20, 2003
All Rights Reserved

Electromagnetic Analysis of Energy System Devices

by
Yan Li

A THESIS

submitted to

Oregon State University

in partial fulfillment of
the requirements for the
degree of

Master of Science

Presented November 20, 2003
Commencement June 2004

Master of Science thesis of Yan Li presented on November 20, 2003

APPROVED:

Co-Major Professor, representing Electrical and Computer Engineering

Co-Major Professor, representing Electrical and Computer Engineering

Director of the School of Electrical Engineering and Computer Science

Dean of the Graduate School

I understand that my thesis will become part of the permanent collection of Oregon State University libraries. My signature below authorizes release of my thesis to any reader upon request.

Yan Li, Author

ACKNOWLEDGEMENTS

First, I would like to express my sincere gratitude to my co-major professors, Dr. Alan Wallace and Dr. Annette von Jouanne, for their guidance, support, and consideration during the time that I have been a part of the energy systems group. I would also like to thank the other members of my program committee, Dr. Huaping Liu and Dr. Charles Brunner, for their willingness to be on my committee and their valuable time and advices.

I would like to thank my fellow students in the energy systems group, who have given me much assistance, motivation and friendship during the past several years, especially Shaoan Dai, Jifeng Han and Andre Ramme.

In addition, I would like to thank Ken Rhinefrank from HP for providing me the opportunity to be involved in their research project and helping me get the approval from HP to include parts of the project achievements in my thesis.

And finally, I would like to thank my family for their ongoing encouragement and support.

TABLE OF CONTENTS

	<u>Page</u>
1. INTRODUCTION.....	1
1.1 Traditional and New Applications of Energy System Devices.....	1
1.2 Background of Electromagnetic Analysis in Energy Systems.....	3
1.3 Objectives and Organization of Thesis	8
2. LTA AND FEM IN EM MODELING	9
2.1 Layer Theory Approach (LTA).....	9
2.2 Finite Element Method (FEM).....	14
2.3 Comparison of LTA and FEM.....	18
3. LAYER MODELING FOR ENERGY SYSTEM DEVICES	19
3.1 Layer Modeling for Permanent Magnet Couplings	19
3.2 Computer Program for Performance Prediction for PM Couplings.....	29
3.3 Performance Prediction for PM Couplings	31
3.4 Comparison of Predicted and Test Data for PM Couplings.....	35
3.5 Parametric Design Study.....	39
3.6 Conceptual Design of a Large “Silent” Brake	42
3.7 Summary	44
4. FEM MODELING FOR THE PROTOTYPE OF A LINEAR RELUCTANCE MACHINE.....	45
4.1 Introduction	45
4.2 FE Modeling for the Linear Reluctance Machine Prototype	47
4.3 FEA Software Maxwell 2D.....	50
4.4 Simulation Results for the Linear Reluctance Machine Prototype	53
4.5 Comparison of Simulation Results and Test Results	57
4.6 FE Modeling for the Production Machine	60
4.7 Summary	64

TABLE OF CONTENTS (Continued)

	<u>Page</u>
5. Conclusions and Suggestions for Future Work.....	65
5.1 Conclusions	65
5.2 Suggestions for Future Work	66
 BIBLIOGRAPHY	 67

LIST OF TABLES

<u>Table</u>	<u>Page</u>
3.1 Parameters of permanent magnet couplings for the layer model program	32
3.2 Parameters of the dynamometer brake for the layer model program.....	32
3.3 Estimated principal dimensions of the magnet coupling brake	44

LIST OF FIGURES

<u>Figure</u>	<u>Page</u>
1.1 Summary of electromagnetic analysis techniques of energy system devices..	7
2.1 Single-sided linear induction machine(SLIM).....	9
2.2 Longitudinal cross-section of the single-sided LIM	10
2.3 Seven-layer model of the single-sided LIM.....	10
2.4 Generalized LIM model with N regions	12
2.5 One dimension boundary-value problem.....	15
2.6 Solution domain (0,1) divided into three subdomains	15
3.1 Adjustable-speed permanent magnet coupling components	19
3.2 Layer model representation of PM couplings	21
3.3 Magnetic circuit model of the permanent magnet with linear demagnetization curve	23
3.4 Equivalent current density for an adjacent magnet pair.....	23
3.5 Dimensions of conducting discs	27
3.6 Flowchart of solution algorithm for the computer program.....	30
3.7 Permanent magnet coupling dynamometer/brake	31
3.8 Prediction and test torque/speed characteristics at six airgap settings.....	33
3.9 Torque/speed characteristics above peak torque conditions	34
3.10 Axial force/speed characteristic (single-side)	35
3.11 Prediction and test torque/speed characteristics at 1 inch airgap.....	36
3.12 Prediction and test torque/speed characteristics at 1/2 inch airgap.....	37
3.13 Prediction and test torque/speed characteristics at 3/8 inch airgap.....	37

LIST OF FIGURES (Continued)

<u>Figure</u>	<u>Page</u>
3.14 Prediction and test torque/speed characteristics at 1/4 inch airgap.....	38
3.15 Prediction and test torque/speed characteristics at 3/16 inch airgap.....	38
3.16 Prediction and test torque/speed characteristics at 3/20 inch airgap.....	39
3.17 Torque/speed characteristics generated in parametric design study(I)	40
3.18 Axial force/speed characteristics generated in parametric design study.....	41
3.19 Torque/speed characteristics generated in parametric design study(II).....	41
3.20 Schematic of the magnetic disc of the large magnetic coupling brake	42
4.1 x-y plane view of prototype demo	45
4.2 x-z plane view of prototype demo.....	46
4.3 x-y plane FE model	47
4.4a x-z plane FE model for 4 extended out cores	49
4.4b x-z plane FE model for 4 extended out laminations with fictitious parts	49
4.5 General procedures of 2-D FEA in Maxwell 2D	52
4.6 User interface window of Maxwell 2D.....	53
4.7 Magnetic flux distribution for x-y plane model	54
4.8 Magnetic flux density distribution for x-y plane model.....	54
4.9 Flux distribution of x-z model with the component at the starting point.....	55
4.10 Flux distribution of x-z model with the component between first pole pair	56
4.11 Flux distribution of x-z model with the component between first and second pole pairs	56
4.12 Calibration based on levitation force in x-y model.....	57

LIST OF FIGURES (Continued)

<u>Figure</u>	<u>Page</u>
4.13 Comparison of simulation and test thrust force/ampere-turn characteristics....	58
4.14 Comparison of simulated and test characteristics of thrust force / component position (Z).....	59
4.15 Channel side-wall force / component position (Z).....	60
4.16 x-y plane model of the production machine.....	61
4.17 x-z plane view of the production machine	61
4.18 x-z plane model of the production machine	62
4.19 Force ratio (F_z/F_x) for the production machine with component#1	63
4.20 Force ratio (F_z/F_x) for the production machine with componet#2	63
4.21 Force ratio (F_z/F_x) for the production machine with component#3	64

ELECTROMAGNETIC ANALYSIS OF ENERGY SYSTEM DEVICES

1. INTRODUCTION

1.1 Traditional and New Applications of Energy System Devices

Electricity is a basic part of nature and it is one of our most widely used forms of energy. We get electricity, which is a secondary energy source, from the conversion of other sources such as coal, natural gas, oil, nuclear power and other natural sources, which are called primary sources. A series of energy system devices such as electrical machines, switching devices, resistors, capacitors and magnetic devices are used to generate, transfer, drive and conserve electric energy. Traditionally, electrical machines are essential for electric energy conversion and supply. They offer a safe, economical and environmentally friendly way both to generate, transmit and distribute electrical energy for various purposes, and to convert electrical energy into mechanical energy through the use of electrical drives and other apparatus. It has been more than 170 years since Michael Faraday succeeded in building the first electric motor in 1831[1]. Nowadays, electric machines are being used in a wide range of areas: industrial applications such as pumps, compressors and fans; transportation applications such as railways and electric vehicles; commercial applications such as elevators and air conditioning; and residential applications such as refrigeration and freezers. Types of classical electrical machines can be categorized generally in terms of the direction of power flow or frequency. Normally, generators are defined as electrical machines that convert mechanical energy into electrical energy, while motors are those that convert electrical energy into mechanical energy. We also can sort electrical machines into DC machines and AC machines. Compared to electrical machines,

other traditional energy system devices such as transformers have simpler operating mechanism since there is only electric energy transferred through an electromagnetic field.

In order to improve the control process and save energy costs in energy systems, new energy system devices such as power semiconductor devices and special electric machines were developed and became widely popular in various applications. In the 1960's, power semiconductor devices i.e. thyristor, GTO (Gate Turn Off) and triac appeared. Power semiconductor devices can help to make energy system devices more compact, more efficient and more flexible to control. One such application of power semiconductor devices is in switched mode power supplies, which can reduce the size of transformers and filter components drastically. Another example for large energy conservation is in motor-driven pump and compressor systems. In a conventional pump system, the pump operates at essentially a constant speed, and the pump flow rate is controlled by adjusting the position of the throttling valve. This procedure results in significant power loss across the valve at reduced flow rates where the power drawn from the utility remains essentially the same as at the full flow rate. This power loss is eliminated by replacing the throttling valve with an adjustable-speed motor drive. By using power semiconductor converter devices motor speeds can be adjusted very efficiently.

In addition, since new materials like rare-earth permanent magnets NdFeB, (neodymium-iron-boron) became commercially available in the 1960's [2], many new energy system devices employing permanent magnets have been developed. Because of their simple structure and high efficiency, these devices have found a wide range of applications. For example, rare-earth permanent magnet machines are widely used in automotive, control, transducer and aerospace applications. In recent years, eddy-current couplings employing high energy-product rare-earth magnets were introduced into industry and found wide range of applications in

large-scale pumps, fans/blowers and compressors [3]. This thesis presents permanent magnet eddy-current coupling research in detail in Chapter 3.

Due to the development of power semiconductor devices, new electrical machines such as linear electric motors and switched reluctance motors have been able to play important roles in many application areas because of their special merits compared to traditional electrical machines. Before the advent of linear electric motors, traditional (rotary) motors with rotary-to-linear converters of some kind were used to produce linear motions. The most obvious advantage of a linear motor is that it has no gears and requires no mechanical rotary-to-linear converters. Thus the linear motor is robust and more reliable. Switched reluctance motors also have advantages of simple and robust structure, low-cost manufacture, and ease in maintenance, repair and replacement. Chapter 4 of this thesis describes the analysis of a linear switched reluctance device with very high leakage components.

1.2 Background of Electromagnetic Analysis in Energy Systems

In 1873, James Clerk Maxwell developed the analytical formulation of electromagnetic radiation and his field equations [4]. For the past two hundred thirty years, the laws of electromagnetism presented by Maxwell have enabled scientists to comprehend and exploit an enormous range of phenomena, and the resulting electromagnetic analysis has become an essential part of many engineering and scientific studies. Electromagnetic theory is valid from the static to optical regimes and from subatomic to intergalactic length scales. The application areas include wireless communication, high-frequency/high-speed circuits and energy systems, etc.

The primary application fields of electromagnetic field analysis in energy systems are for electromagnetic devices such as transformers, electrical machines, and power electronics devices. During processes of designing these devices, electromagnetic field analyses are used to aid design and get products with higher efficiency, higher reliability, more compact size and lower costs which are strongly

requested by customers nowadays. For example, in the field of power plant equipment, such as turbines, we make positive use of numerical simulations on super computers or high performance workstations instead of design methods based on usual empirical or experimental data. Electromagnetic field analysis gives us high performance products. In that sense, it is a very important design tool.

The problem of electromagnetic analysis is actually a problem of solving a set of Maxwell's equations subject to given boundary conditions. Maxwell's equations are a set of fundamental equations that govern all macroscopic electromagnetic phenomena. The equations can be written in both differential and integral forms. The general differential forms are given by [5]

$$\nabla \times E = -\frac{\partial B}{\partial t} \quad (\text{Faraday's law}) \quad (1.1)$$

$$\nabla \times H = \frac{\partial D}{\partial t} + J \quad (\text{Ampere's law}) \quad (1.2)$$

$$\nabla \cdot D = \rho \quad (\text{Gauss's law}) \quad (1.3)$$

$$\nabla \cdot B = 0 \quad (\text{Gauss's law--magnetic}) \quad (1.4)$$

$$\nabla \cdot J = -\frac{\partial \rho}{\partial t} \quad (\text{Equation of continuity}) \quad (1.5)$$

Where,

E = electric field intensity (volts/meter)

D = electric flux density (coulombs/meter²)

H= magnetic field intensity (ampere/meter)

B = magnetic flux density (webers/meter²)

J = electric current density (ampere/meter²)

ρ = electric charge density (coulombs/meter³)

Equation (1.5) that can be derived from (1.2) and (1.3) is the mathematical form of the law of the conservation of charge.

Equation (1.1)--(1.5) are valid in all circumstances regardless of the medium and the shape of the integration volume, surface, and contour. They can be

considered as the fundamental equations governing the behavior of electromagnetic fields.

Among the five equations above, only three are independent for the case of time-varying fields and thus are called the independent equations. Either the first three equations, (1.1)--(1.3), or the first two equations, (1.1) and (1.2), with (1.5) can be chosen as such independent equations. The other two equations, (1.4) and (1.5) or (1.3) and (1.4), can be derived from the independent equations and thus called auxiliary or dependent equations.

When the field quantities of magnetic vector potential, magnetic flux density and magnetic field intensity are obtained, other related parameters such as inductance, capacitance and performances of the analyzed devices can be derived. There are generally two types of solutions for the electromagnetic field problems: one is analytical, and another is numerical. Analytical solutions show more apparently the relations between related parameters and field quantities. We can use them to analyze the effects of parameters on field intensities directly. Layer theory approach (LTA) is one of the analytical methods, which was employed in this thesis to analyze a type of new energy system device, the eddy-current permanent magnet coupling. Due to the complexity, many of electromagnetic field problems for energy system devices cannot be solved with analytical methods. It is needed to make some special simplifications to deal with current sources and boundary conditions. For example, the method of images, which is a way of finding the fields produced by charges in the presence of dielectric or conducting boundaries with certain symmetries, and the method of fictitious currents are used to represent the effects of partial or whole medium on boundary conditions. Also, current sources may be resolved into their Fourier harmonic components in order to obtain solutions of the field equations. Other techniques such as the method of conformal transformation [6] are very complicated and are applicable for special and specific problems.

Numerical methods are adopted widely to solve electromagnetic field problems today with the easy access to powerful computers. It is possible to solve all the electromagnetic field problems by using numerical problems since computers today have faster speeds and larger computing memory. There are generally three kinds of numerical methods: finite difference method, finite element method and method of moments. Finite difference method and finite element method are based on differential equations while method of moment is based on integral equations. Finite difference method is a simple and efficient method for solving ordinary differential equations (ODEs) in problem regions with simple boundaries. The method requires the construction of a mesh defining local coordinate surfaces. For each node of this mesh, the unknown function values are found, replacing the differential equations by difference equations, i.e.

$$dy = f(x, y)dx \text{ is replaced by } \Delta y = f(x + \Delta x / 2, y + \Delta y / 2) / \Delta x ,$$

where Δx , Δy are steps in an iterative procedure.

The finite element method is a powerful method for solving partial differential equations (PDE) in problem regions with complicated boundaries, if the PDE is equivalent to the minimization problem for a variational integral. The method requires the definition of elementary volumes, for each of which the integral can be approximated as a function of node values of the unknown functions. The sum of these variational integral values will be minimized by the method as a function of the node values. The finite element method has become a powerful tool for the numerical solution of a wide range of engineering problems. More introductions of finite element method are given in Chapter 2.

The related process for analysis and performance predictions of electromagnetic devices involving the solution of Maxwell's equations by layer theory approach (LTA) and finite element method (FEM) are shown schematically in Fig.1.1.

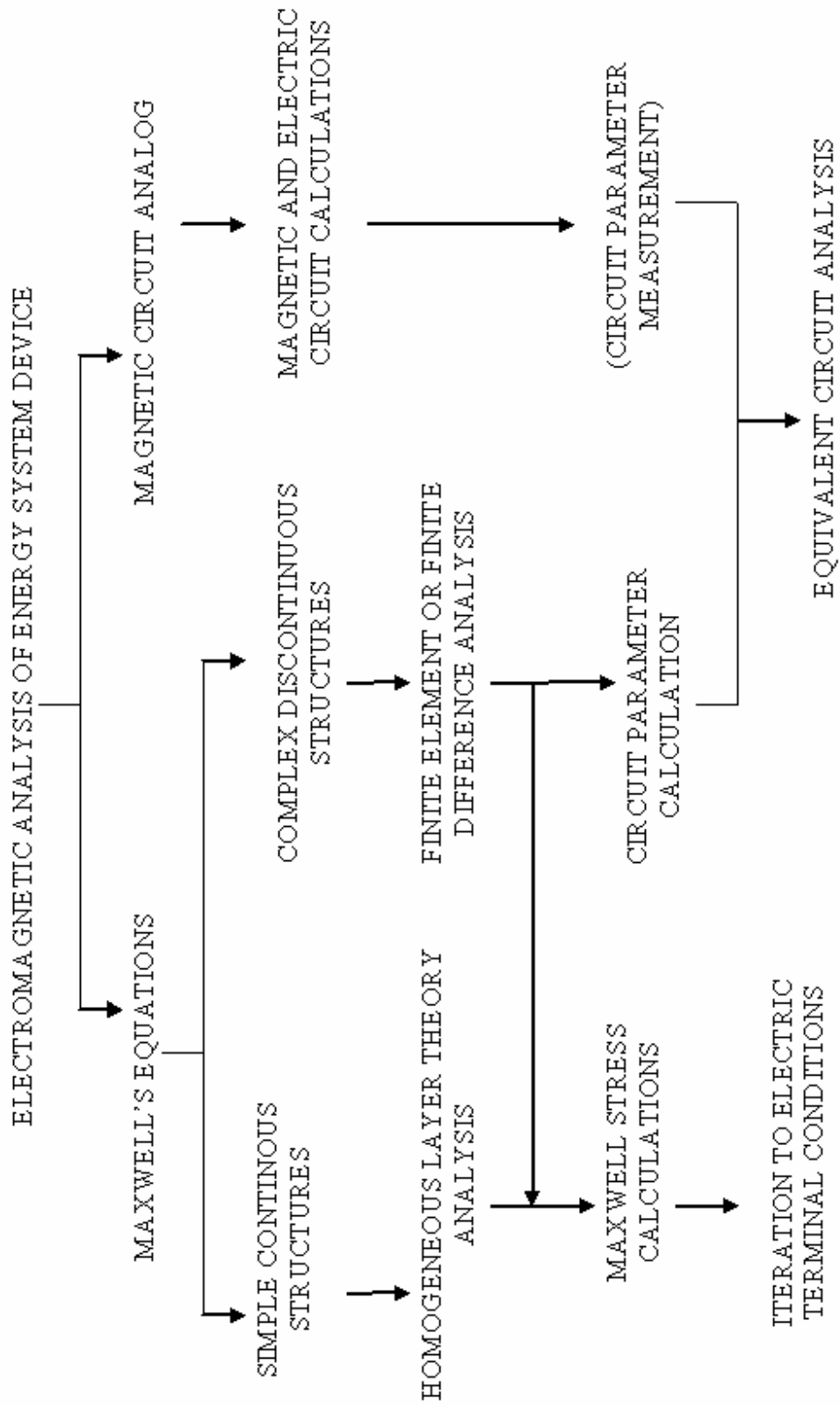


Fig. 1.1 Summary of electromagnetic analysis techniques of energy system devices

1.3 Objectives and Organization of Thesis

The objective of this research work is to apply electromagnetic analysis to do design and performance studies for some energy system devices more efficiently and economically using specially developed computer software and commercial EMA (Electromagnetic Analysis) software.

The thesis is organized according to the following description of chapters. Chapter 1 provides a short overview of applications of energy system devices and background information on electromagnetic analysis approaches. The objective of the thesis research work is also defined.

Chapter 2 focuses on introducing the two primary EMA (electromagnetic analysis) methods adopted in the thesis research work. One is LTA (Layer Theory Approach), and another is FEM (Finite Element Method).

Chapter 3 presents in detail the layer modeling work of an adjustable airgap permanent magnet coupling (PMC) and its derivatives. Comparisons are made between experimental results and simulation results for the PMC.

In Chapter 4, a specific linear reluctance motor design with FEA (Finite Element Analysis) aid is described.

Finally, Chapter 6 presents the conclusions. Also, future work opportunities are surveyed.

2. LTA AND FEM IN EM MODELING

2.1 Layer Theory Approach (LTA)

Layer theory approach was originally developed to analyze the performance of linear machines [7]. It is an efficient analytical EM (electromagnetic) method for performance prediction and design studies of some energy system devices specifically those that include sheet conductor as secondaries. As shown in Fig.2.1, the single-sided linear induction motor (SLIM) consists of a flat primary and a long sheet secondary. Due to the effects such as longitudinal end effects and field diffusion etc., the normal lumped-parameter circuit theory method is difficult to apply and not an accurate approach for this type of device. This difficulty is also due to problems of representing sheet conductor by equivalent resistance and

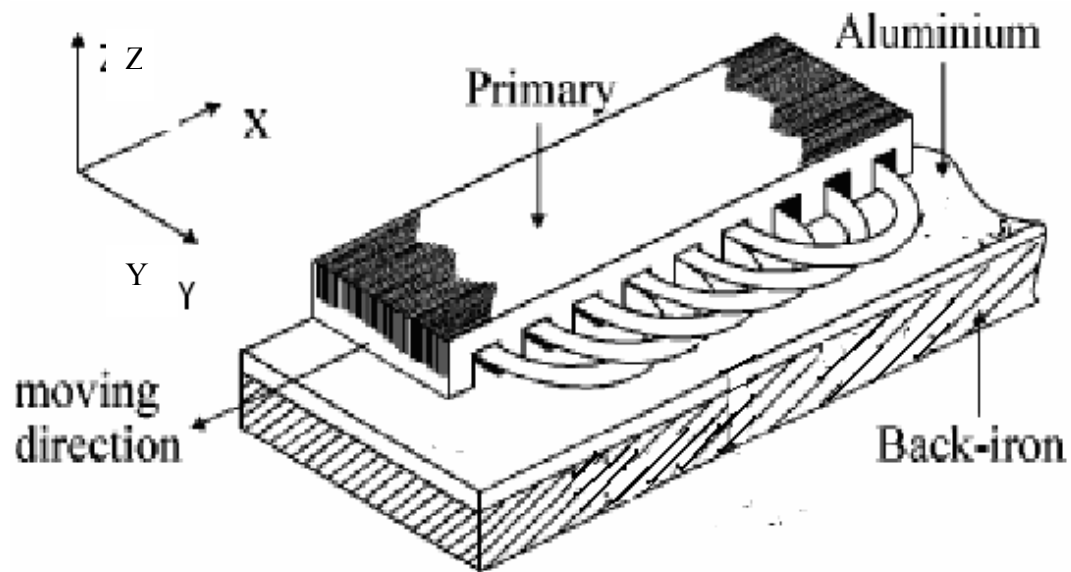


Fig. 2.1 Single-sided linear induction machine (SLIM)

reactance, which in practice shows high slip dependency. As one of the distributed-parameter field theory methods, layer theory approach (LTA) is a relatively

straightforward and accurate and efficient method compared to other field theory methods like finite element method. Fig. 2.2 shows the 2-D longitudinal cross-section of the SLIM. The 2-D seven-layer model of one pole pitch of the cross-section is as shown in Fig.2.3. Since the yoke and the teeth have different magnetic

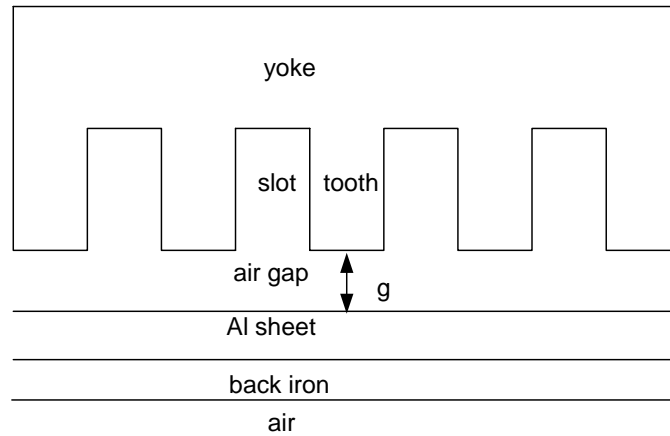


Fig. 2.2 Longitudinal cross-section of the single-sided LIM

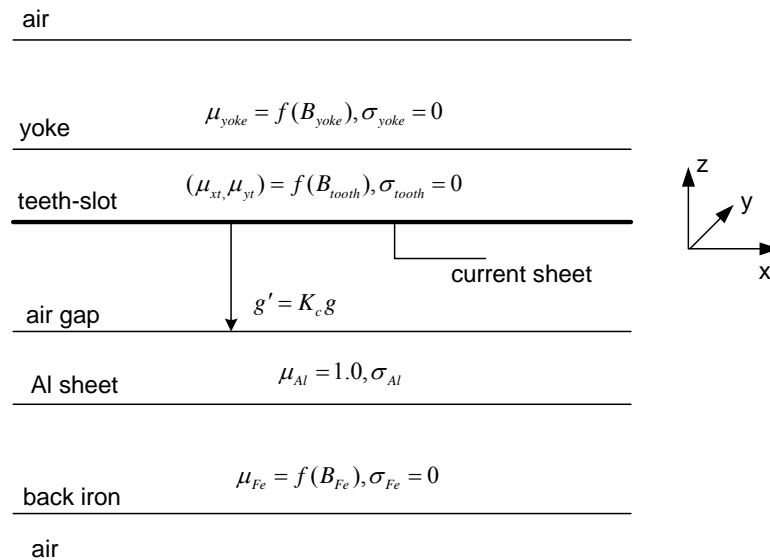


Fig. 2.3 Seven-layer model of the single-sided LIM

states related to saturation and the combination of tooth and slot has different conductivity and permeability from the yoke area, the structure of the iron teeth and air slot uses a division of the primary into two separate regions. One region is a homogeneous yoke layer having a field dependent permeability μ_{yoke} and another is an equivalent teeth-slot layer having an isotropic field dependent permeability defined by its x and z components (μ_{xt} , μ_{zt}). The model is assumed continuous in the y direction and calculations are initially based on lengths of a meter in that axis. These two regions are assumed to have zero conductivity in the x-z plane. The winding is represented by an infinitely thin current sheet (J), and the actual slotted armature has been replaced by a smooth structure by introducing Carter's coefficient (K_c), which modifies the actual airgap g to an effective value g_e [8]. The secondary consists of two layers that represent a double layer reaction rail comprising a high conductivity aluminum cap over a laminated ferromagnetic core having a field dependent permeability μ_{Fe} . In addition, the SLIM is bounded by two infinite half planes representing the air above and below the machine. Thus, the entire machine is modeled by seven layers in which each layer represents a specific region of the actual machine. To analyze the performance of the SLIM more practically and efficiently, a generalized mathematical formulation of a multilayer SLIM model is developed. Each layer is characterized by its conductivity σ_i , relative permeability in the x and z directions to allow for anisotropy, μ_{xi} , μ_{zi} , and thickness d_i . The current sheet lies between layers (r) and (r-1). Regions (1) and (N) are assumed to extend to $-\infty$ and to $+\infty$, respectively, in the z direction. In the case of linear induction machines, the layer (r+1) to (N) represent the regions within the secondary component and are assumed to move at a constant velocity U. The field equations are established for the generalized layer model as shown in Fig.2.4. Based on Maxwell's equations, the equations describing the vector potential A inside any conducting and anisotropic layer is given by

$$\bar{\nabla} \times (\bar{\mu}^{-1}(\bar{\nabla} \times \bar{A})) = \sigma \left[-\frac{\partial \bar{A}}{\partial t} + \bar{U} \times (\bar{\nabla} \times \bar{A}) \right] \quad (2.1)$$

In 2-D analysis, $\bar{\mu}^{-1}$ has the following form:

$$\bar{\mu}^{-1} = \begin{bmatrix} \frac{1}{\mu_x} & 0 \\ 0 & \frac{1}{\mu_z} \end{bmatrix} \quad (2.2)$$

To simplify the above equation, three assumptions can be made in this case:

- (i) The relative motion of the linear induction motor component is assumed to be in the x-direction only. i.e. $U = \frac{dx}{dt}$
- (ii) All the currents are constrained to flow in the y-direction only. This implies that $J = J_y \cdot \hat{a}_y$ and $A = A_y \cdot \hat{a}_y$
- (iii) Time variations are sinusoidal; i.e. A is of the form $A(x, y, z) = A(z) \exp[j(\omega t - \beta x)] \hat{a}_z$

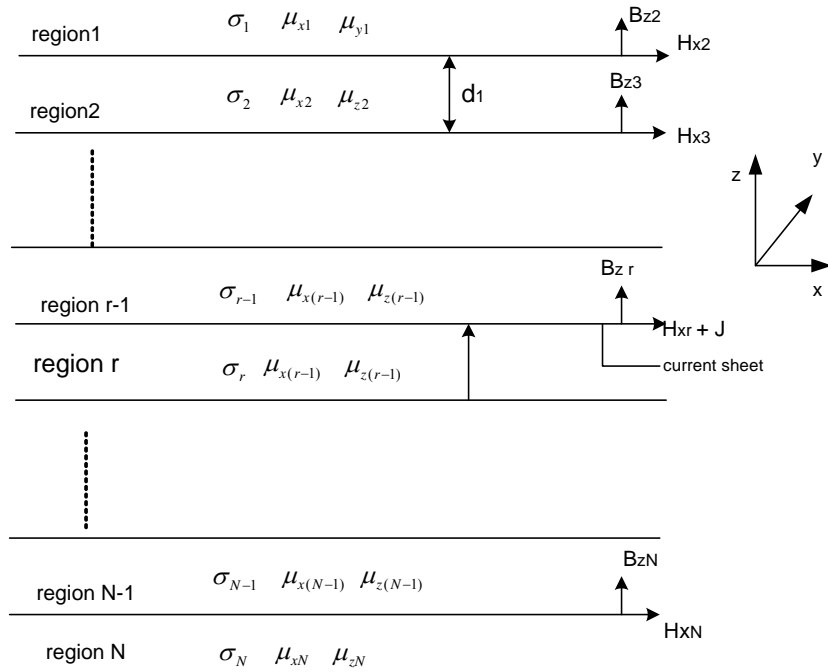


Fig. 2.4 Generalized LIM model with N regions

Consequently, the basic simplified governing equation that must be satisfied in each layer of the LIM model becomes as follows

$$\frac{1}{\mu_{xi}} \frac{\partial^2 A_{yi}}{\partial z^2} + \frac{1}{\mu_{zi}} \frac{\partial^2 A_{yi}}{\partial x^2} = \sigma_i \left(j\omega A_{yi} + U_{xi} \frac{\partial A_{yi}}{\partial x} \right) \quad (2.3)$$

In addition, the boundary conditions are as follows:

- (a) B_y is continuous
- (b) All field components disappear at $y=\pm\infty$
- (c) If a current sheet, J , lies between two layers (i) and (i+1) then

$$H_{x(i+1)} - H_{xi} = J$$

When solutions for vector potential A are obtained, the magnetic flux density and magnetic intensity can be determined from:

$$\nabla \times A = B \quad (2.4)$$

$$H = \frac{B}{\mu} \quad (2.5)$$

Then the performance of the LIM can be calculated. The induced current density in any given region of the secondary is formulated as

$$J_{yi} = \sigma_i \left(-\frac{\partial A_{yi}}{\partial t} - U_x \frac{\partial A_{yi}}{\partial x} \right) \quad (2.6)$$

The time-average force densities in the x and y directions are derived from the basic Lorentz force equation

$$f_{xi} = -0.5 \operatorname{Re}(J_{yi} B_{yi}^*) \quad (2.7)$$

$$f_{zi} = -0.5 \operatorname{Re}(J_{yi} B_{xi}^*) \quad (2.8)$$

where B_{xi}^* and B_{yi}^* are the conjugate values of the x and y component of the flux density, and Re indicates the real component of the product.

2.2 Finite Element Method (FEM)

The finite element method (FEM) has its origin in the field of structural analysis. Although the earlier mathematical treatment of the method was provided by Courant in 1943, the method was not applied to EM problems until the 1960s. The idea of utilizing the finite element method for electromagnetic field analysis draws its roots in 1968 in the pioneering work of Winslow [9]. In spite of its short period of implementation in the field of electromagnetics, the finite element method has been successfully applied to the analysis of various problems in electromagnetics in the last nearly forty years including analysis of electrostatic and magnetostatic fields, eddy-current problems, high-frequency problems, electromagnetic scattering and wave propagation phenomena, etc. Today, the finite element method has widely established procedure for analysis, optimization and design of electromagnetic devices and a large portion of modern CAD (Computer Aided Design)/CAM (Computer Aided Manufacture)/CAE (Computer Aided Engineering) modules or expert systems are partially or entirely based on this method.

The basic procedure of the traditional finite element method is to divide the domain under investigation, either being one-dimensional (1-D), two-dimensional (2-D) or three-dimensional (3-D) domain, into a finite number of simple subdomains or elements (e.g. short line segments in 1-D, triangles in 2-D or tetrahedral in 3-D domain) and then to approximate the unknown variable in each sub-domain by an interpolating polynomial that is continuous with its derivative until a certain order. The values of the unknown variable at each node of such an established network of subdomains (elements), usually called a finite element mesh, are the objective of the analysis. In the next step, by using the node values of each primitive (e.g. triangle), and the previously established piecewise approximation functions, the values of the unknown function at each point inside the domain of analysis can be easily computed.

Here, we use a simple boundary-value problem as an example to introduce the finite element method [10]. The specific problem to be considered is determination of the static potential ϕ between two infinite parallel plates as shown in Fig. 2.5.

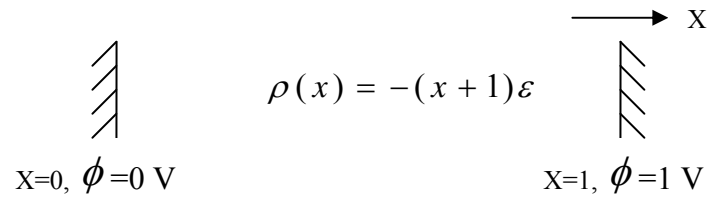


Fig. 2.5 One dimension boundary-value problem

One plate is located at $x=0$ with $\phi=0 \text{ V}$ and the other is located at $x=1$ with $\phi=1 \text{ V}$. The space between the plates is filled with a medium having a constant permittivity ϵ and a varying electric charge density $\rho(x) = -(x+1)\epsilon$. This problem can be described mathematically by the simplified Poisson equation:

$$\frac{d^2\phi}{dx^2} = x+1 \quad 0 < x < 1 \quad (2.9)$$

In order to apply finite element method to solve this problem, first, we divide the entire solution domain $(0,1)$ into three subdomains (as shown in Fig. 2.6) defined by (X_1, X_2) , (X_2, X_3) , and (X_3, X_4) , with X_1 and X_4 being the endpoints, i.e. $X_1=0$



Fig. 2.6 Solution domain $(0, 1)$ divided into three subdomains

and $X_{4=1}$. The other two points can be chosen as $X_2=1/3$ and $X_3=2/3$ or other arbitrary appropriate values. We assume the trial function as a linear variation of $\phi(x)$ over each subdomain defined by

$$\tilde{\phi}(x) = \phi_i \frac{x_{i+1} - x}{x_{i+1} - x_i} + \phi_{i+1} \frac{x - x_i}{x_{i+1} - x_i} \quad (2.10)$$

for $x_i \leq x \leq x_{i+1}$ and $i=1,2,3$, where the ϕ_i are unknown constants to be determined. From the boundary conditions, we find $\phi_1 = 0$ and $\phi_4 = 1$. To determine the remaining unknown constants ϕ_2 and ϕ_3 , we use either the Ritz variational or the Galerkin method. In the Ritz method we formulate the problem in terms of a functional whose minimum corresponds to the differential equation under the given boundary conditions. For the example problem, it can be shown that the functional is given by

$$F(\tilde{\phi}) = \frac{1}{2} \int_0^1 \left(\frac{d\tilde{\phi}}{dx} \right)^2 dx + \int_0^1 (x+1)\tilde{\phi} dx \quad (2.11)$$

And we substitute (2.10) into (2.11) to find that

$$F = \sum_{i=1}^3 \left[\frac{1}{2} \int_{x_i}^{x_{i+1}} \left(\frac{\phi_{i+1} - \phi_i}{x_{i+1} - x_i} \right)^2 dx + \int_{x_i}^{x_{i+1}} (x+1) \left(\phi_i \frac{x_{i+1} - x}{x_{i+1} - x_i} + \phi_{i+1} \frac{x - x_i}{x_{i+1} - x_i} \right) dx \right] \quad (2.12)$$

Evaluating the integrals, we obtain

$$F = \sum_{i=1}^3 \frac{1}{2} (x_{i+1} - x_i) \left[\left(\frac{\phi_{i+1} - \phi_i}{x_{i+1} - x_i} \right)^2 + \phi_{i+1} \left(\frac{2}{3} x_{i+1} + \frac{1}{3} x_i + 1 \right) + \phi_i \left(\frac{2}{3} x_i + \frac{1}{3} x_{i+1} + 1 \right) \right] \quad (2.13)$$

which can be written as

$$F = 3\phi_2^2 + 3\phi_3^2 - 3\phi_2\phi_3 + \frac{4}{9}\phi_2 - \frac{22}{9}\phi_3 + \frac{49}{27}$$

(2.14)

after substitution of the values of x_i , ϕ_1 and ϕ_4 . To minimize F, we take the partial derivatives of F with respect to ϕ_2 and ϕ_3 and set them to zero. This gives

$$\frac{\partial F}{\partial \phi_2} = 6\phi_2 - 3\phi_3 + \frac{4}{9} = 0 \quad (2.15)$$

$$\frac{\partial F}{\partial \phi_3} = -3\phi_2 + 6\phi_3 - \frac{22}{9} = 0 \quad (2.16)$$

for which we obtain

$$\phi_2 = \frac{14}{81} \quad \text{and} \quad \phi_3 = \frac{40}{81}$$

The above results can also be obtained by Galerkin's method, which seek the solution by weighting the residual of the differential equation. For further and detailed descriptions we can refer to [9-11].

The basic procedure of finite element method is as described in this example and can be summarized in the following:

- i) Discretization or subdivision of the domain
- ii) Selection of the interpolation function
- iii) Formulation of the system of equations
- iv) Solution of the system of equations

2.3 Comparison of LTA and FEM

As indicated before, the layer theory approach is an analytical method and the finite element method is a numerical method for solving electromagnetic (EM) problems. The layer theory approach is more straightforward and efficient in application than finite element method. It requires less computing time and computing memory. Also its solutions can show more apparently the relations between related parameters and field quantities. However, its application is limited to devices which possess, or can be readily approximated to, simple or special structures. Many devices with complicate structures are not readily solved using the layer theory approach due to their complexity and lack of accuracy required by the simplifying assumptions. The finite element method has wider application areas than the layer theory approach. It can be applied to most kinds of problems even with complicated structure and boundaries, either in 1-D, 2-D or 3-D models. The solutions obtained can be sufficiently accurate for practical application requirements. However, much longer computing times and larger computing memory are required by finite element analysis work, especially for 3-D FEM. In conclusion, both the layer theory approach and the finite element method are very powerful tools for electromagnetic analysis of energy system devices. It depends on features of practical problems and the solution requirements to decide which method to choose. The following chapters will investigate two very useful, but structurally different devices that illustrate the relative values of the layer theory approach and the finite element method.

3. LAYER MODELING FOR ENERGY SYSTEM DEVICES

3.1 Layer Modeling for Permanent Magnet Couplings

3.1.1 Introduction

In 1998, a range of permanent magnet couplings was introduced into the industrial drives market [12]. As shown in Fig. 3.1, the permanent magnet coupling normally consists of two sets of components. Discs containing sets of alternatively polarized high-energy magnets are connected to the load. Copper conducting discs

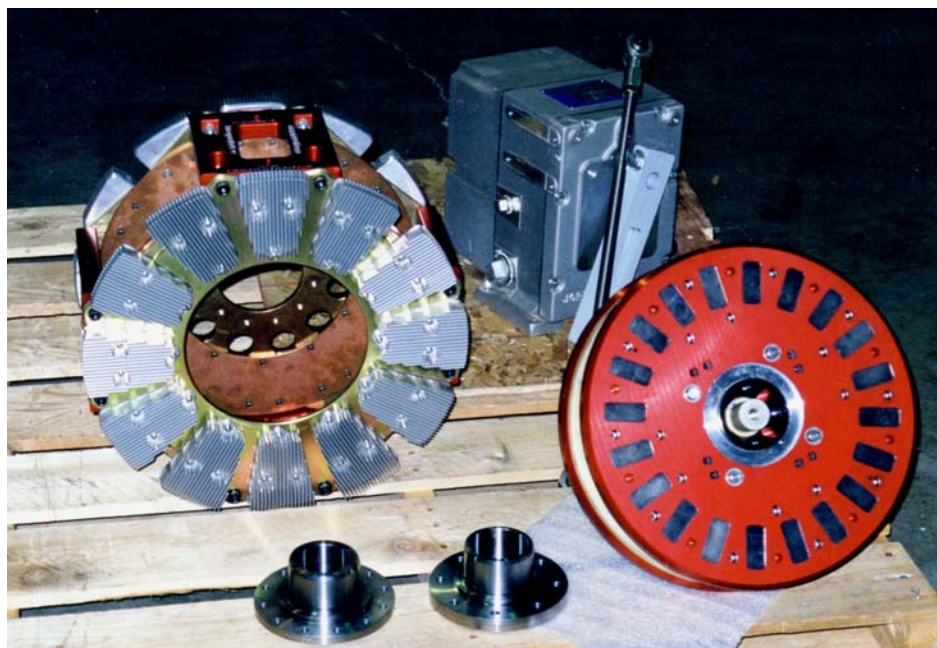


Fig. 3.1 Adjustable-speed permanent coupling components

opposing the magnets, are attached to the motor. The operating principle of permanent magnet couplings is relatively straightforward. It utilizes the relative motion between the magnets and conducting discs to induce eddy currents which develop torques and normal forces between these two components. As a result, the torque is transmitted from the motor to the load across the airgap between the two discs. The net normal (axial) force acting along the motor and load shafts will be

equal and opposite for a symmetrical coupling. Couplings with fixed-gap configuration have been marketed worldwide [12]. They provide several advantages over conventional mechanical couplings such as providing mechanical isolation of motor and load, enabling soft-start, tolerating a degree of misalignment of shafts, alleviating vibrations and disturbances originating in the load, and enabling electrical isolation that can prevent circulation of potentially harmful bearing currents between motors and loads. In recent years, in order to meet customers' requirements of energy savings and lower costs for new equipment installation, more development work has focused on adjustable air-gap versions of these couplings. Two major devices have been explored: the dynamometer brake and the adjustable speed coupling system (ASCS). In the adjustable speed coupling system, the magnet discs are moved along the load shaft by an internal screw activating a cam on the mounting system. So the airgap between the magnets and the conducting disc can be continuously adjusted while the coupling is in operation. In the dynamometer brake system, the magnetic discs are axially adjustable as in the adjustable speed coupling while the conductor discs are axially and radially fixed to dissipate all the power input to the system and function as a brake. The adjustable speed coupling system (ASCS) provides a variable-speed drive without the use of power electronics. It is reported that the adjustable speed coupling system (ASCS) can provide 25% to 66% audited energy savings in various installations such as pumps, fans and blowers [13].

The design of devices like permanent magnet couplings is mainly undertaken using a blend of experiences, extrapolation and trial-and-error. It is a time consuming and potentially expensive process. In order to speed up the design process, save prototype cost and help optimize existing products, a linear field analysis layer model which is suitable for these couplings including sheet conductor as secondaries, has been developed and demonstrated.

3.1.2 Layer Model of Permanent Magnet Coupling

In the linear layer model, the permanent magnet coupling is treated as being cut radially and rolled out flat in the circumferential direction. This enables the rectangular co-ordinate system to be adopted for the modeling process. Fig. 3.2 shows the basic layer model of permanent magnet (PM) couplings. The following reasonable assumptions are made on the model [14]:

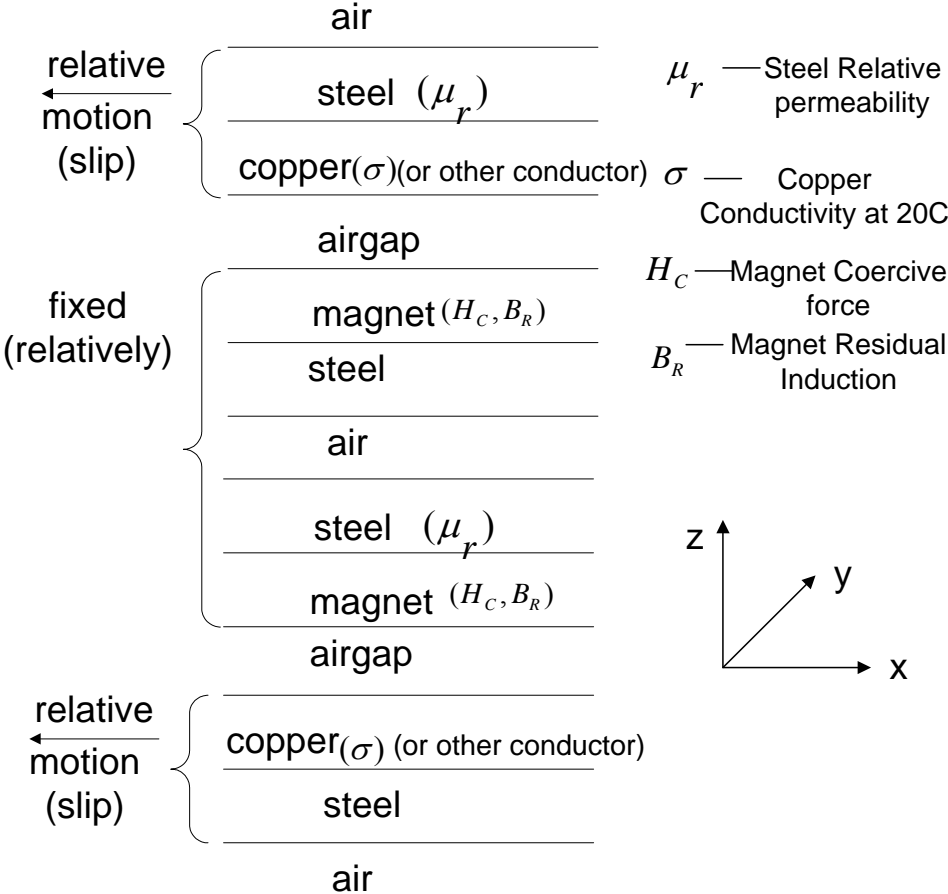


Fig. 3.2 Layer model representation of PM couplings

1. All layers are assumed to be homogeneous and all field quantities are constant in the y-direction.

2. Conductivity σ and constant relative permeability μ_r are used to define the properties of non-excitation layers (copper and steel layers).
3. The excitation layers (magnets) are assumed to have a linear demagnetization characteristic and are represented by an equivalent current sheet.
4. Temperature effects are considered using simple thermal coefficients.
5. The excitation layers (magnets) are assumed to be static. The conductor layers (copper and its backing steel layer) are assumed to be moving at linear velocity v with respect to the magnets.
6. Each permanent magnet disc is assumed to be faced by a conductor disc on either side. So only one pair of magnet and conductor discs are simulated. Any additional disc pairs then are considered to be replications of the first pair of discs.

3.1.2.1 Excitation layer representation

The magnetic disc with a linear demagnetization characteristic is represented with an equivalent current sheet. Based on ampere's law, the effective mmf (magnetomotive force) F of the magnet is given by

$$F = H_c l_m = I \quad (3.1)$$

where,

H_c is the coercive force of the magnet (as shown in Fig. 3.3)

l_m is the axial depth (z-direction) of the magnet

I is the equivalent current

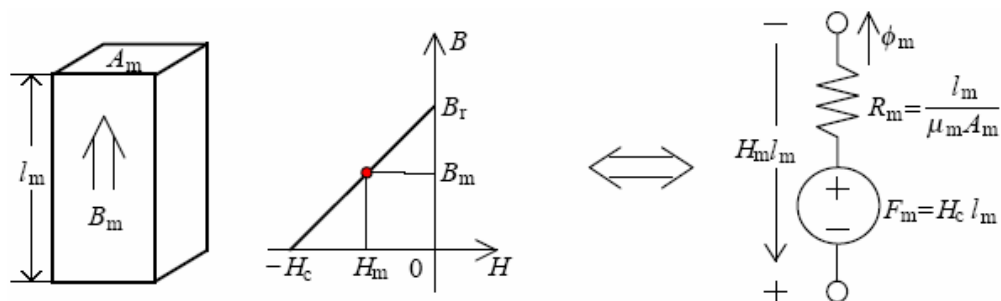


Fig. 3.3 Magnetic circuit model of the permanent magnet with linear demagnetization curve

In Fig. 3.3,

A_m is the magnet cross-sectional area

μ_m is the relative permeability of the magnet

B_m is the magnetic flux density in the magnet

Then the equivalent current density distribution $J_y(x)$ for an adjacent magnet pair is shown in Fig. 3.4. The equivalent current density distribution is odd symmetrical at $x=x_0$.

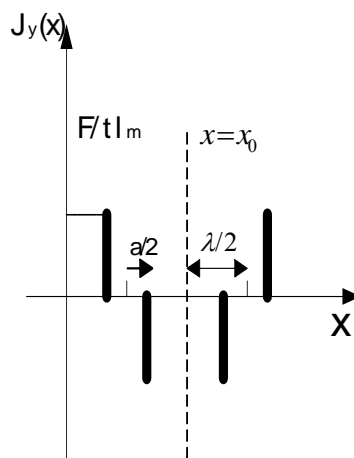


Fig. 3.4 Equivalent current density for an adjacent magnet pair

where,

F is magnetomotive force as defined in equation. (3.1)

t is the thickness of equivalent current sheet

l_m is the axial depth of the magnet

a is the circumferential width of the magnet

λ is the magnet pitch

If it is assumed that the distribution repeats periodically with each pair of adjacent magnets, we can resolve the current density distribution $J_y(x)$ into a harmonic Fourier series expressed in complex notation as in equation (3.2),

$$J_y(x) = \sum_{k=-\infty}^{\infty} J_{mk} e^{-jkx} \quad (3.2)$$

where,

$$k = \frac{iN_m}{y_m} \quad (\text{period} = \frac{\pi y_m}{N_m}) \quad (3.3)$$

i is the normal harmonic number and N_m is the total number of magnets

y_m is the mean magnet diameter on the disc (as shown in Fig. 3.5)

If we assume the finite thickness of the equivalent current (t_m) can be ideally reduced to zero and the choice of x_0 is arbitrary, the magnitude of fourier series component is given by

$$J_{mk} = \left(\frac{2 F N_m}{\pi y_m l_m} \right) \sin \left(\frac{k a}{2} \right) \sin \left(\frac{i \pi}{2} \right) \quad (3.4)$$

where,

i is a series of positive and negative odd integers ($\pm 1, \pm 3, \pm 5, \dots$)

F, N_m , y_m , l_m , k and a are the same as defined before.

In the layer model, the magnet disc is assumed to be held stationary. So the field equation for the magnetic disc is developed in the stationary reference frame. Based on the assumptions made before, the following rules are applied:

$$H_y = E_x = E_z = 0 \quad (3.5)$$

So, the tangential field intensity H_x and normal flux density B_z are chosen as the field variables in Maxwell's equations, which have the general solution written in matrix form as:

$$\begin{bmatrix} H_n \\ \frac{J_{mk}}{k} - j \frac{B_n}{\mu_n} \end{bmatrix} = \begin{bmatrix} \sinh(k S_n) & \cosh(k S_n) \\ \cosh(k S_n) & \sinh(k S_n) \end{bmatrix} \begin{bmatrix} \frac{J_{mk}}{k} - j \frac{B_{n-1}}{\mu_n} \\ H_{n-1} \end{bmatrix} \quad (3.6)$$

where,

k is same as defined before.

H and B represent the k th components of H_x and B_z .

n represents the upper surfaces of the magnet layer.

$n-1$ represents the lower surfaces of the magnet layer.

S_n represents the thickness of n th layer.

Equation (3.6) can be simplified as equation (3.8) using the concept of field surface admittance:

$$R_n = \frac{H_n}{B_n} \quad (3.7)$$

$$B_n = \frac{J_{mk}}{k} \left[\frac{R_{n-1} (\cosh k S_{n-1}) + \frac{1}{j \mu_n} \sinh k S_n}{\left(R_n R_{n-1} + \frac{1}{\mu_n^2} \right) \sinh k S_n + \frac{1}{j \mu_n} (R_n - R_{n-1}) \cosh k S_n} \right]$$

(3.8)

3.1.2.2 Non-excitation layer representation

The conductor layers and their backing layers are assumed to have a velocity v (as given in equations (3.1)) in the stationary reference frame. We can transfer to a moving reference frame [14]:

$$e^{jkx} \rightarrow e^{j(kvt-kx')} \quad (3.9)$$

From this it can be developed that, for surfaces n and $n-1$ of the layer n in motion,

$$B_n = B_{n-1} \cosh \alpha_n S_n + j \frac{k \mu_n}{\alpha_n} H_{n-1} \sinh \alpha_n S_n \quad (3.10)$$

$$H_n = \frac{\alpha_n}{j k \mu_n} B_{n-1} \sinh \alpha_n S_n + H_{n-1} \cosh \alpha_n S_n$$

where,

$$\alpha_n^2 = k_n^2 + j kv \sigma_n \mu_n \quad (3.11)$$

v is the motion velocity of the moving layers.

σ is the conductivity of the non-excitation layers.

μ is the permeability of the non-excitation layers.

In order to take into account the eddy current induced in the conduction layer which flows in the x -direction (i.e., copper overhang and underhang regions), the Russell and Norsworthy coefficient k_d [15] is adopted in order to revise the natural local conductivity σ_0 ,

$$\sigma = k_d \sigma_0 \quad (3.12)$$

where,

$$k_d = 1 - \frac{\tanh\left(\frac{\pi b}{\lambda 2}\right)}{\frac{\pi b}{\lambda 2} \left[1 + \tanh\left(\frac{\pi b}{\lambda 2}\right) \tanh\left(\frac{\pi c}{\lambda}\right) \right]} \quad (3.13)$$

in which,

b represents the radial depth of the magnet.

c represents the overhang or underhang of the conducting disc, which is given by

$$c_o = \frac{1}{2}(y_o - y_m - b) \quad \text{and} \quad c_u = \frac{1}{2}(y_m - y_i - b) \quad (3.14)$$

c_o is the conductor overhang and c_u is the conductor underhang, and the dimensions of conducting discs are described in Fig. 3.5.

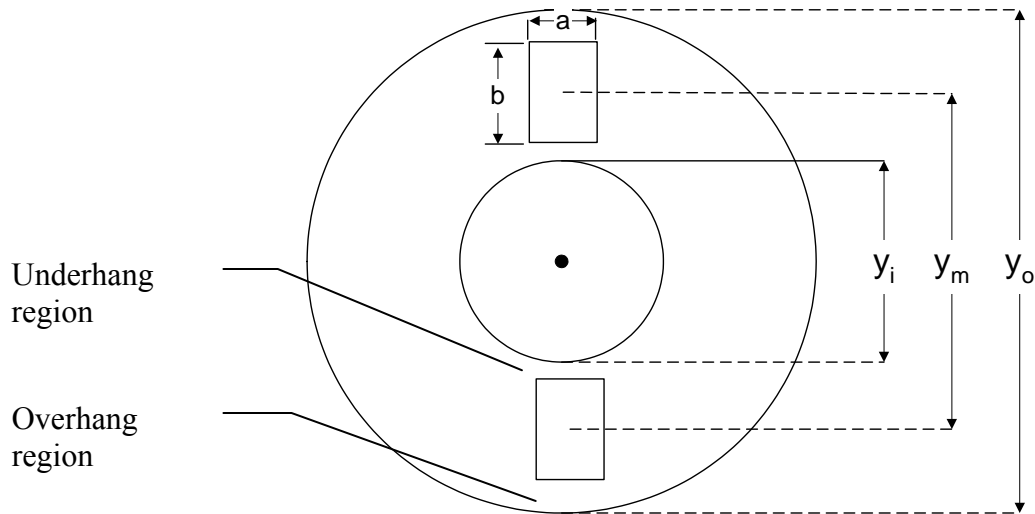


Fig. 3.5 Dimensions of conducting discs

As before, to simplify the solution of the field equations (3.10), the concept of surface admittance R is defined again,

$$R_n = \frac{\frac{\alpha_n}{j k \mu_n} \tanh \alpha_n S_n + R_{n-1}}{1 + \frac{j k \mu_n}{\alpha_n} R_{n-1} \tanh \alpha_n S_n} \quad (3.15)$$

$$R_{n-1} = \frac{R_n - \frac{\alpha_n}{j k \mu_n} \tanh \alpha_n S_n}{1 - \frac{j k \mu_n}{\alpha_n} R_n \tanh \alpha_n S_n} \quad (3.16)$$

Specially, for the surface admittance at the outer air boundary is determined as equation (3.17) because the fields in those regions are assumed to decay to zero exponentially with the distance z .

$$R_{air} = \frac{1}{j \mu_o} \quad (3.17)$$

3.1.2.3 Performance analysis

The objective of the layer modeling work described above is to predict performance of the adjustable airgap/speed coupling system. After the field quantities like flux density and field intensity are solved throughout the field equations, the torque and normal forces at any layer boundary can be calculated. Normally the regions that are focused on are at the airgap/conductor boundary. According to the Maxwell stress tensor, the transmitted torque is given by [14]

$$T = \frac{b y_m^2 \pi}{2} \sum_{k=-\infty}^{\infty} B_{ck} H_{ck}^* \quad (3.18)$$

in which,

B_{ck} is the k^{th} harmonic component of axial flux density.

H_{ck} is the k^{th} harmonic component of tangential field intensity.(where the subscript c denotes the conduction layer).

* denotes a conjugate quantity

the axial force is given by

$$F_z = \frac{b y_m \pi}{2} \sum_{k=-\infty}^{\infty} \left\{ \frac{|B_{ck}|^2}{\mu_c} - \mu_c |H_{ck}|^2 \right\} \quad (3.19)$$

Based on the above layer model and all the field equations presented for the permanent magnet coupling systems, a simple and efficient computer program can be developed to aid the product design and optimization [14].

3.2 Computer Program for Performance Prediction for PM couplings

The solution algorithm of the computer program is presented using the flowchart as shown in Fig. 3.6. The program was developed using the FORTRAN language which has powerful numerical and high-performance computing capabilities. It is a straightforward process to run the program.

First, we need to set the required parameters referring to the practical type of the coupling. Generally, there are four types of permanent magnet couplings: fixed airgap couplings, adjustable gap/adjustable speed couplings, rapid disconnect couplings and dynamometer brake couplings. For example, to simulate a dynamometer brake type of the permanent magnetic coupling as shown in Fig. 3.7, besides the geometric sizes of the magnets and the conducting discs and the material field properties of the magnets and copper, we need to set the field

properties of the backing layer for the conducting disc. Specifically, since a water cooling system is used for conducting discs, the backing layer is water that has unity relative permeability.

Second, after compiling the program and the input data file manually input the slip speed range referring to the rated speed of the motor and analysis needs.

Third, check the output data files for simulation results such as torques and normal forces.

Finally, if a parametric design study is needed, reset the parameters in the input data file.

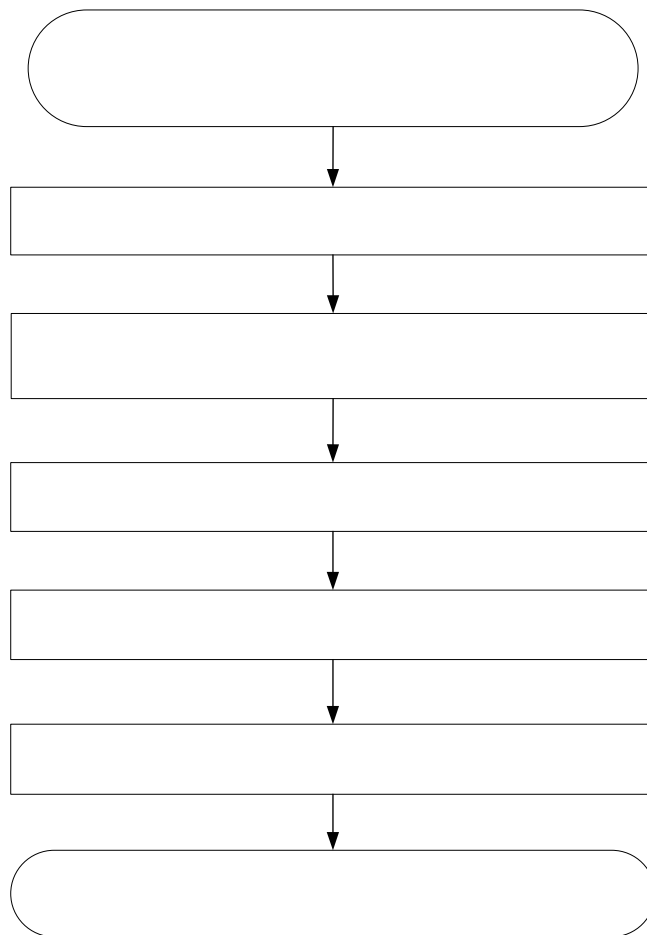


Fig. 3.6 Flowchart of solution algorithm for the computer program

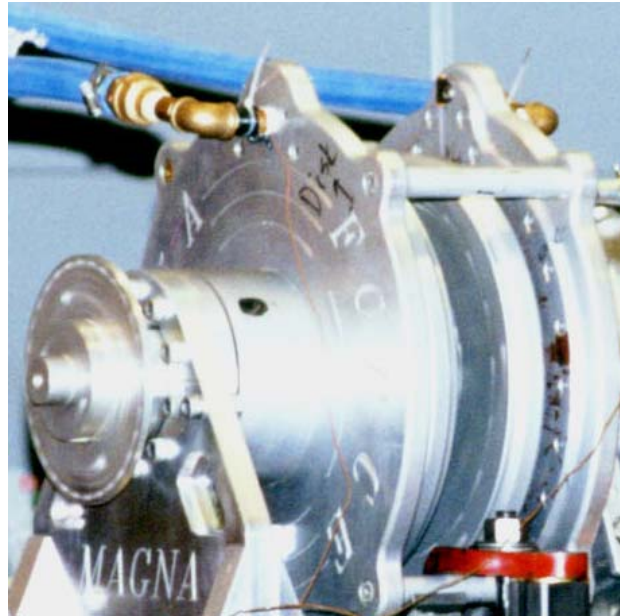


Fig. 3.7 Permanent magnet coupling dynamometer/brake

3.3 Performance Prediction for PM Couplings

The basic performance characteristics of interests for permanent magnet couplings are the torque vs. slip speed characteristic and the axial force vs. slip speed characteristic. These two characteristics are functions of the dimensions of the coupling device and properties of the materials in the particular layers. Table 3.1 shows the main parameters required by the layer model program. For a specific existing adjustable-airgap coupling product, the dimensions and material properties are fixed. Only the airgap between the magnet disc and the conductor disc and temperature are variable. Table 3.2 shows dimensions and parameters of the studied adjustable-airgap dynamometer-brake coupling produced by MagnaDrive. The layer model program is used to predict its performance for six different airgap settings, which demonstrates the inverse airgap relationship for torque for all speeds above the peak torque conditions. The predicted torque/speed characteristics are shown in Fig. 3.8.

Table 3.1 Parameters of permanent magnet couplings for the layer model program

Fixed device dimensions	parameters	Fixed material properties
Conductor disc axial thickness	airgap	Conductor disc conductivity
Backing disc axial thickness	temperature	Backing disc permeability
Disc diameter at center of magnets		Magnet coercivity
Magnet sizes		Magnet residual flux density
Total number of magnet		

Table 3.2 Parameters of the dynamometer brake for the layer model program

Conductor backing disc axial thickness (mm)	None (water cooling)
Conductor disc axial thickness (mm)	7.62
Airgap axial thickness (mm)	Variable in range 3.18 to 25.4
Magnet axial thickness (mm)	25.4
Magnet backing disc thickness (mm)	6.35
Outer overhang of conductor disc (mm)	31.11
Inner overhang of conductor disc (mm)	31.11
Mean magnet diameter (mm)	279.4
Magnet radial depth (mm)	50.8
Magnet circumferential width (mm)	25.4
Conductor backing disc relative permeability	1
Magnet backing disc relative permeability	500 (steel)
Conductor conductivity at 20°C (Siemens/M)	5.8×10^7
Disc operating temperature	Refer to test data
Magnet residual inductance (T)	1.25
Magnet coercive force, (A/m)	9.5×10^5
Total number of magnets	20

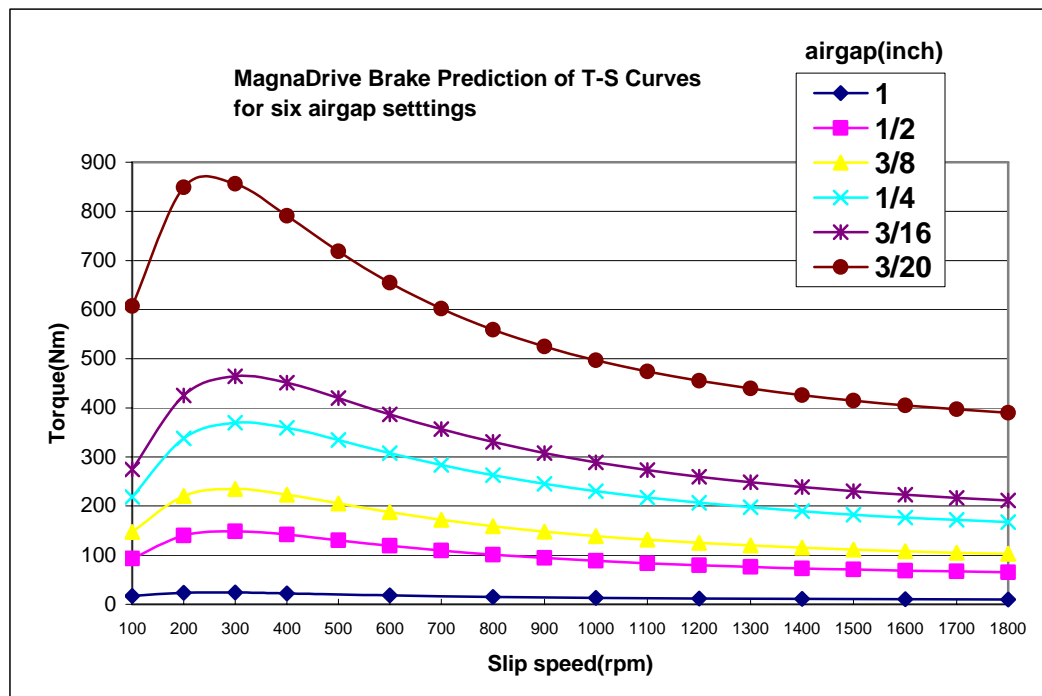


Fig. 3.8 Prediction and test torque/speed characteristics at six airgap settings

Based on this series of torque/speed curves in Fig. 3.8, the peak torque is observed to be at around 300rev/min. Another series of torque/airgap curves as a function of different slip speeds can be generated as shown in Fig. 3.9, which demonstrates the inverse relationship between the torque and airgap.

The axial force/slip speed characteristic for a single side of the dynamometer-brake coupling is also shown in “w/o back steel disc” curve of Fig. 3.9. It can be observed that there is no axial force when slip speed equals zero. The reason is that conductor discs of the dynamometer-brake coupling do not have backing steel discs, there are no constant attractive forces that magnets produce on backing steel discs. There are only axial forces that magnets produce on eddy currents induced in conductor discs. The axial force curve when the coupling has backing discs is also shown in Fig. 3.9 for comparison. Normally, the coupling is symmetrical and the axial forces on the two conductor discs are equal and opposite. So the axial force

characteristics are not as critical as torque characteristics for the coupling performance.

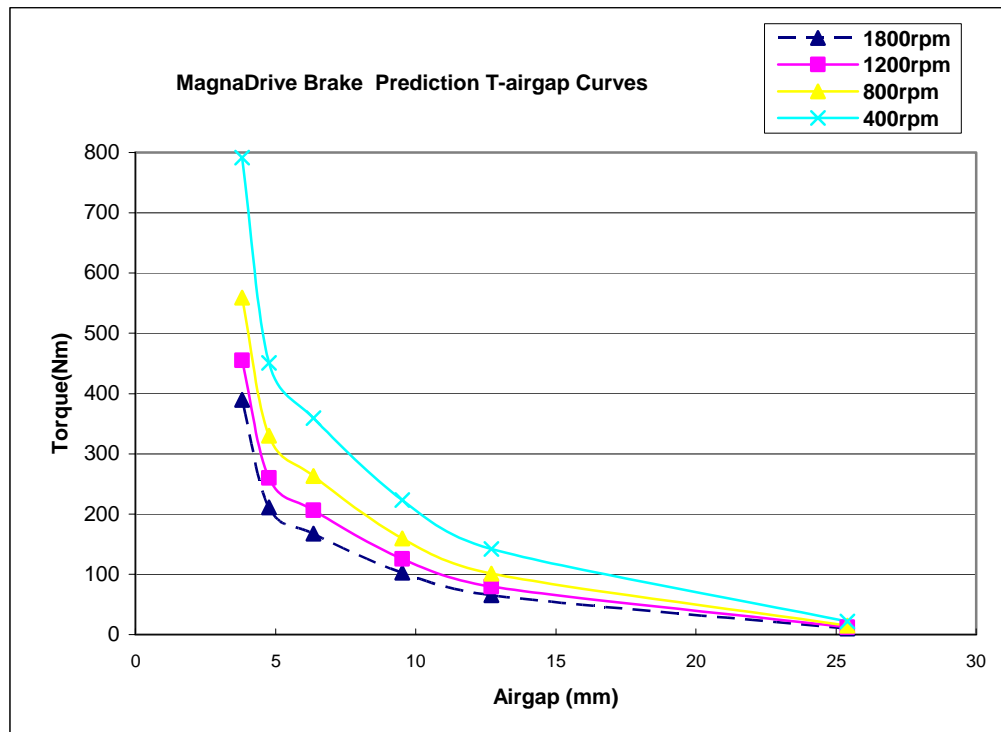


Fig. 3.9 Torque/speed characteristics above peak torque conditions

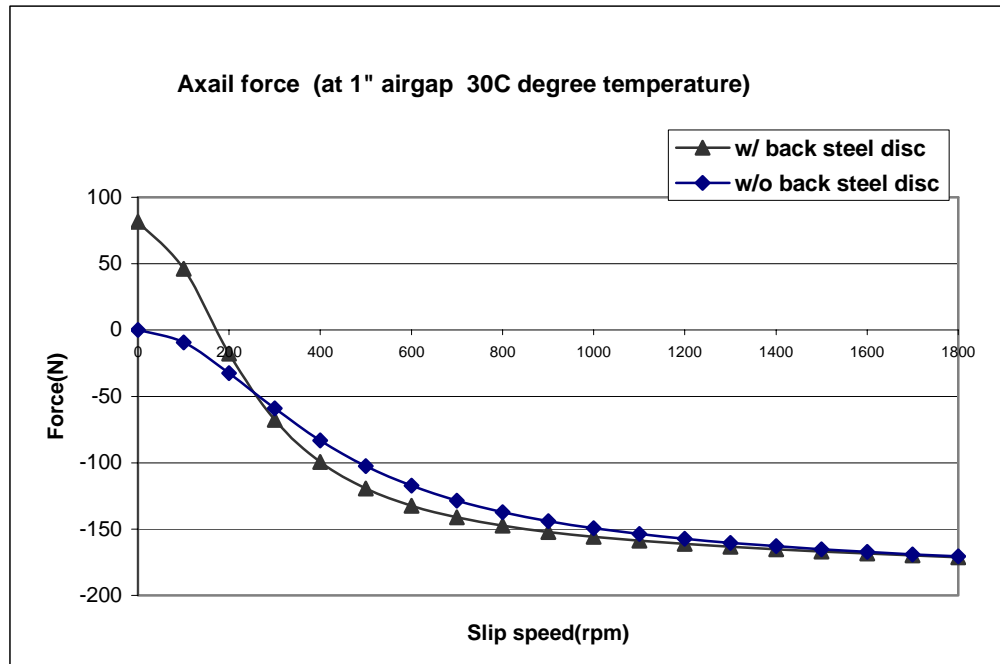


Fig. 3.10 Axial force/slip speed characteristic (single-side)

3.4 Comparison of Predicted and Test Data for PM Couplings

To investigate the validity of the layer model program, the prediction results and test data for torque/speed characteristics of the adjustable-airgap dynamometer brake are compared as shown in Fig.3.11-Fig.3.16. The comparison shows that:

- 1) For all six airgap settings, the layer model predicts the peak torque occurs at a lower slip speed (300rev/min) than the measured slip speed (400rev/min). The predicted torque is generally smaller than measured torque at high slip speed.
- 2) The difference between the predicted peak torque and measured peak torque at the smallest airgap is bigger than the differences at other larger airgaps.

- 3) The main cause for the differences is the approximation of 3-D effects in the model. Other possible reasons are temperature effects and a higher magnetic saturation for the smaller airgap.
- 4) Overall, the layer model prediction has good correlation with test data considering the assumptions made in applying the model.

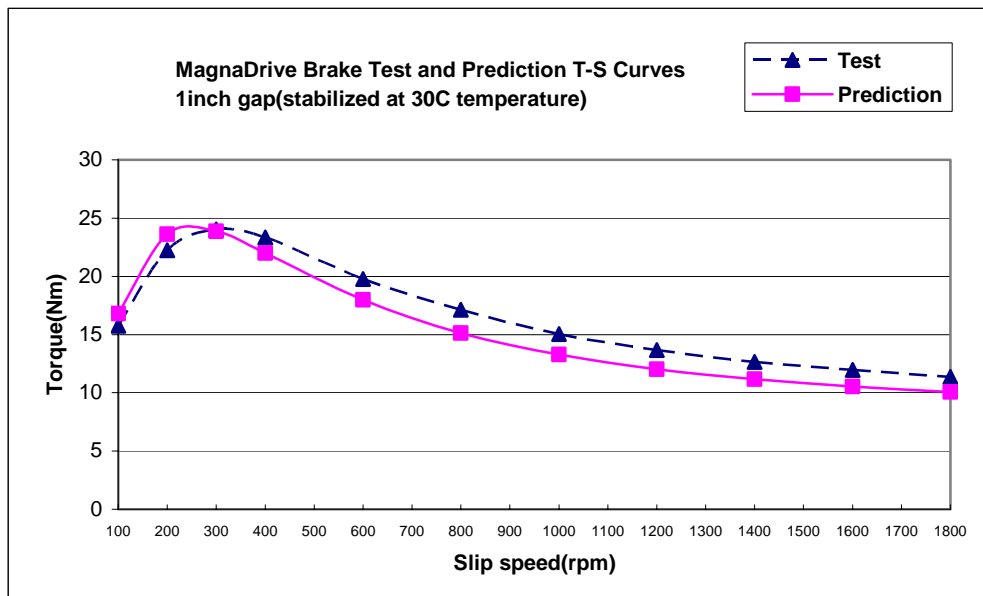


Fig. 3.11 Prediction and test torque/speed characteristics at 1 inch airgap

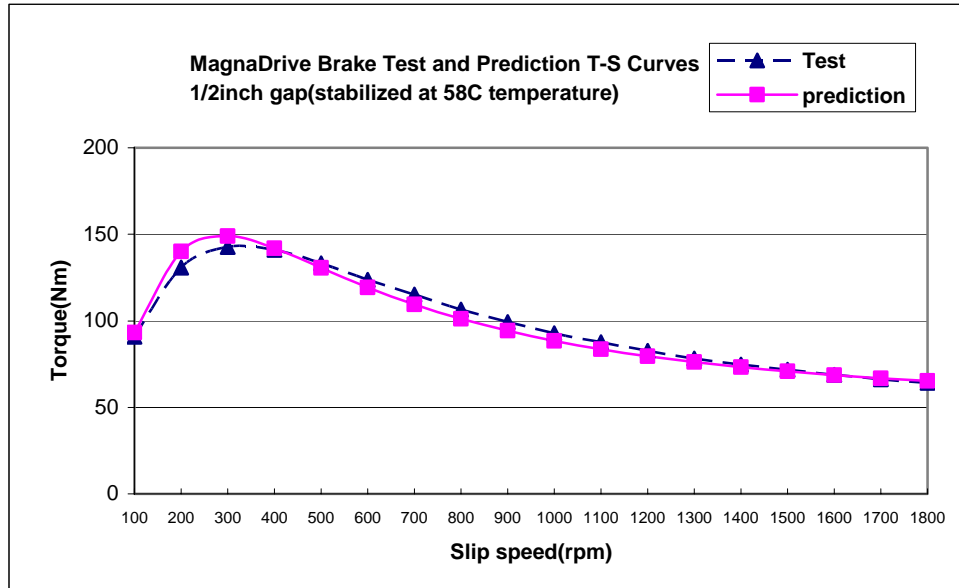


Fig. 3.12 Prediction and test torque/speed characteristics at 1/2 inch airgap

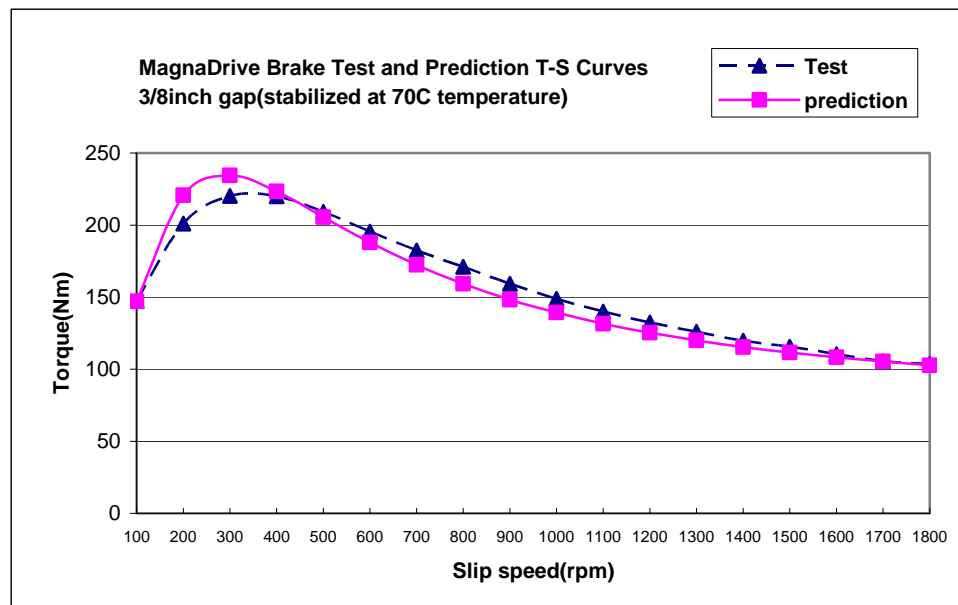


Fig. 3.13 Prediction and test torque/speed characteristics at 3/8 inch airgap

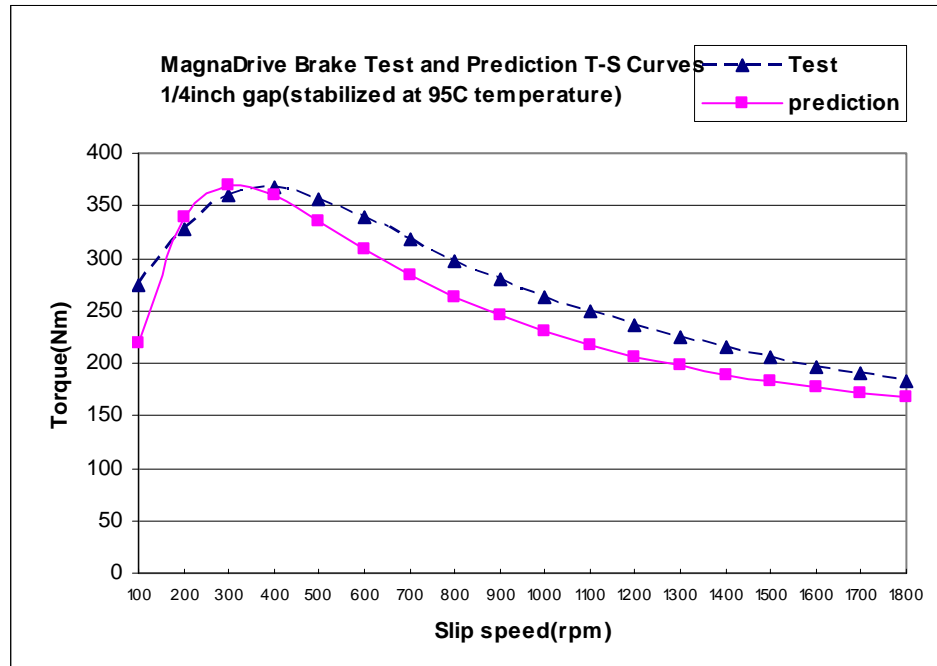


Fig. 3.14 Prediction and test torque/speed characteristics at 1/4 inch airgap

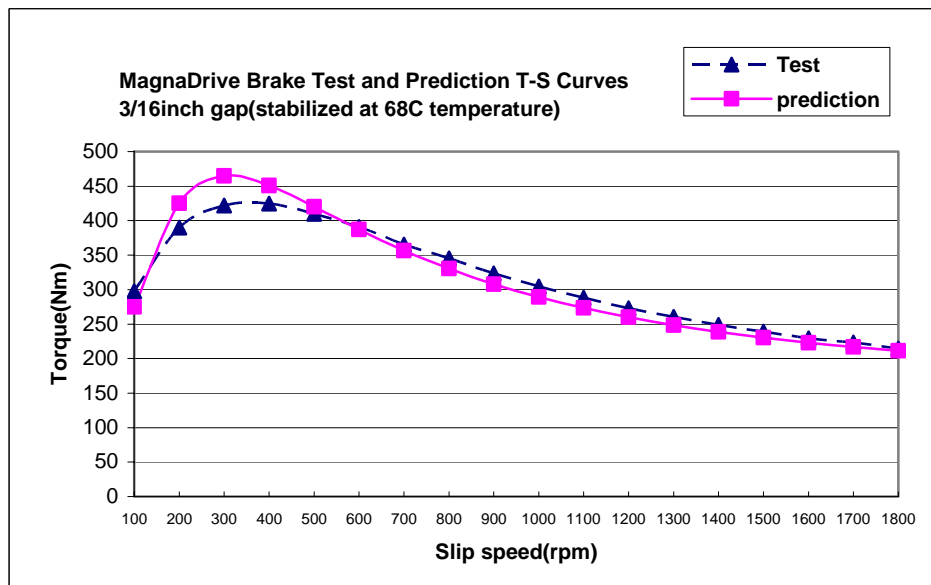


Fig. 3.15 Prediction and test torque/speed characteristics at 3/16 inch airgap

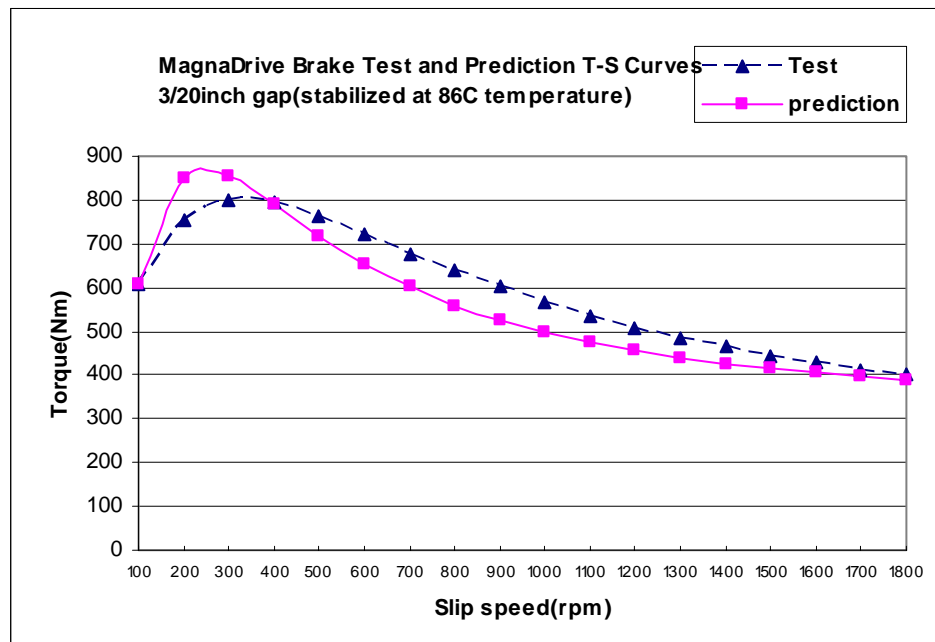


Fig. 3.16 Prediction and test torque/speed characteristics at 3/20 inch airgap

3.5 Parametric Design Study

Because of the advantages of low computing memory requirements, short computing time and sufficient accuracy, the layer theory model of an existing permanent magnet coupling is suitable to use as a parametric design tool to aid the optimization of existing coupling products and develop new products. All the dimensions and material properties can be chosen as variable parameters during the design study based on the objective of optimization and performance requirements. The basic parameters that can be chosen include:

- a) Conductor sheet thickness
- b) Conductor backing sheet thickness
- c) Magnet sheet thickness
- d) Magnet backing sheet thickness

- e) Airgap
- f) Number of magnets
- g) Size of magnets

This thesis conducted some preliminary work for a parametric design study. Fig. 3.17 and Fig. 3.18 show, respectively, the torque/speed and axial force/speed characteristics of an adjustable speed coupling while choosing copper discs thickness as the variable. They show that torque and axial forces increase as the copper disc thickness increases, and that the slip at which both maximum torque and the reversal of the direction of normal (axial) forces decreases as copper conductor thickness increases. This is consistent with expectations based on a comparison with induction motors. In Fig. 3.19, a series of torque/speed curves were generated for an adjustable speed coupling while choosing conductor disc conductivity as variable. It can be observed that the peak torque occurs at lower slip speed when conductor conductivity increases. Based on these studies and performance requirements, the manufacturer can make some optimization decisions to chose materials that save costs while keeping required performance satisfactory.

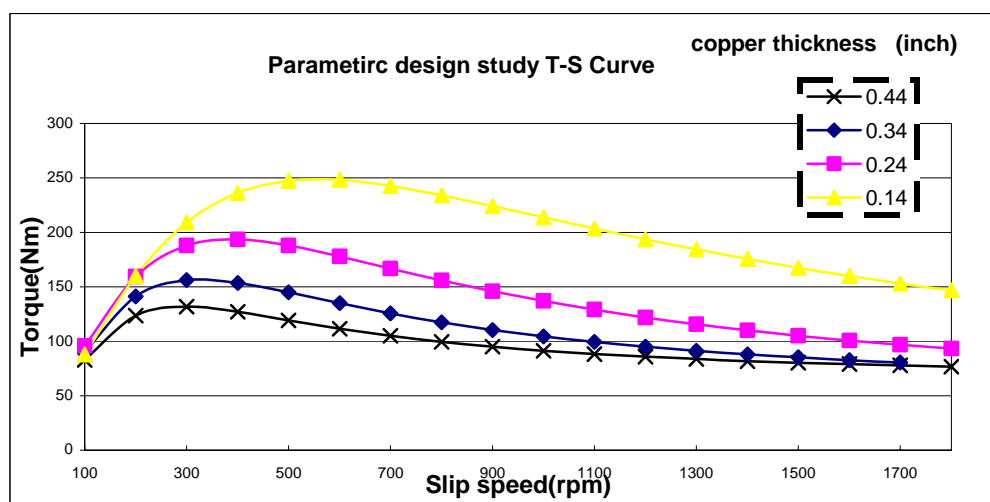
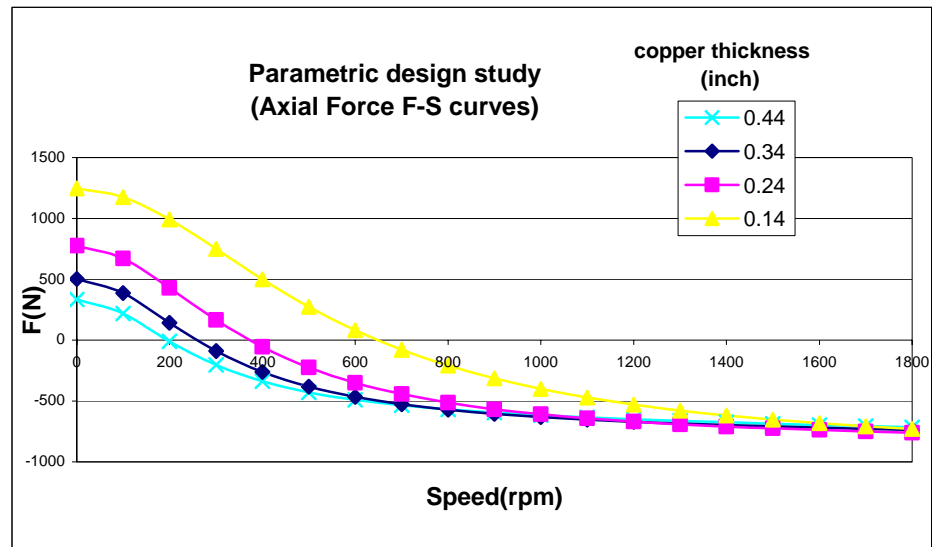


Fig.3. 17 Torque/speed characteristics generated in parametric design study (I)



F. 3.18 Axial force/speed characteristics generated in parametric design study

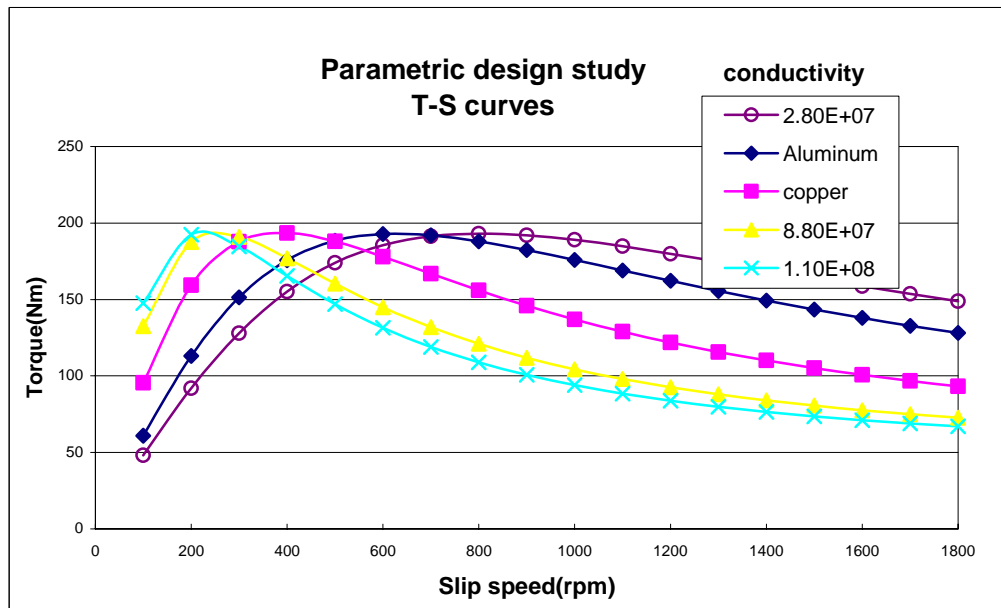


Fig. 3.19 Torque/speed characteristics generated in parametric design study (II)

3.6 Conceptual Design for a Large “Silent” Brake

A device which has been derived from the magnetic coupling is an eddy-current brake that provides controllable contact-free braking without wearing components. Consequently, this concept is considered a superior type of large and quiet brake. The US Navy currently has several projects in process to develop the concept of an “all electric ship”. The propulsion motors for these future ships are currently being developed and tested. One of the critical features of these high power motors is the acoustic noise signature (particularly for

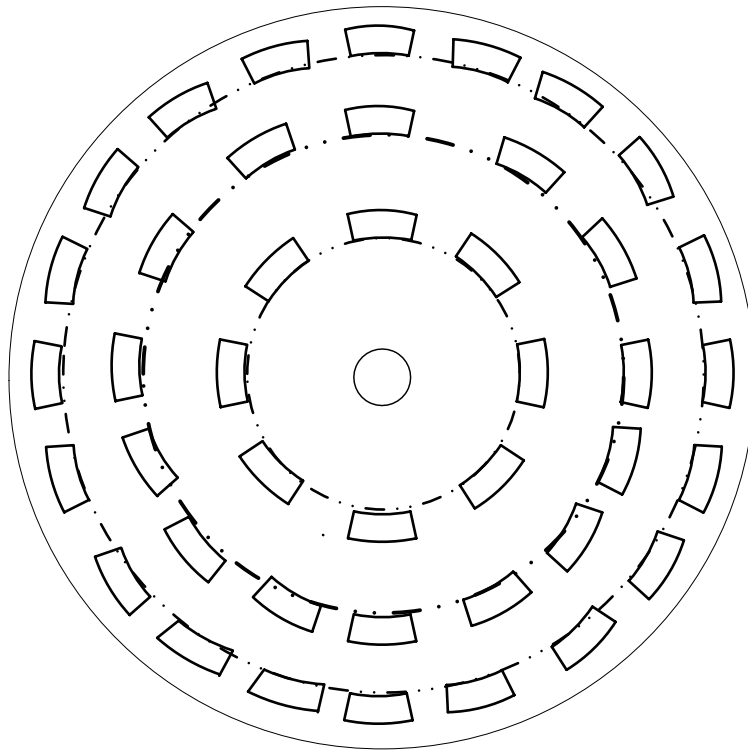


Fig. 3.20 Schematic of the magnetic disc of the large magnetic coupling brake

submarines). Consequently there is a need to test these motors, by loading them to rated limits and measuring the sound level produced. In such an application, an eddy-current brake is appropriate because of its mechanical isolation and the vibration and disturbance alleviation between motor and load. The energy absorption of the brake can be external to the acoustic chamber in which the motors are being tested. Braking energy can be transmitted through the chamber wall by the high-strength permanent magnets. With the layer approach theory model, the conceptual design of a permanent magnet coupling with 5MW rated braking power that provides 207,600 Nm of braking

torque at 230 rpm speed, was investigated. Due to the high power and torque ratings, the size of this coupling will be extremely large if we use the traditional configuration in which the magnets comprise a single set placed peripherally on the disc. In order to limit the size of this large brake, a new configuration of the magnetic disc was proposed as shown in Fig. 3.20. There are three sets of magnets placed at three different radii of the disc. The effective torque of the coupling is the sum of torques generated by relative motions between three sets of magnets and the conductor disc. The preliminary simulation results from the layer model program can estimate the principal dimensions of the magnetic coupling brake.

Table 3.3 shows estimated principle dimensions for the magnet coupling brake using the copper conductor disc outside the chamber to meet the application requirements. Other alternate materials: aluminum and bronze are also investigated. The 1.9cm (0.75 inch) airgap was chosen to give sufficient design tolerance between the magnet disc and conductor disc. With more application requirements available in the future, more detailed characterizations can be simulated and analyzed, in order to provide the “quiet” brakes needed.

Table 3.3 Estimated principal dimensions of the magnet coupling brake

Principal dimensions		Torque at slip speed 230rpm (Nm)	Power rating (MW)
Mean magnet diameter (cm)	508/406/305 (3 sets)		
Magnet sizes(cm)	10.16×20.32×5.08		
Conductor(copper) disc thickness (cm)	5.08		
Magnet backing disc thickness (cm)	5.08		
Conductor backing disc thickness (cm)	5.08		
Airgap (cm)	1.90		
Conductor material (conductivity Siemens/m)	Copper (5.8×10^7)	2.12×10^5	5.1
	Aluminum (3.42×10^7)	2.60×10^5	6.2
	Bronze (1.16×10^7)	3.20×10^5	7.7

3.7 Summary

This chapter presents the modeling and performance prediction for an dynamometer brake coupling with LTA (Layer Theory Approach). For the devices that have been constructed and tested, the prediction results have good correlation with test data. Also, some preliminary design study work and the conceptual design of a large quiet magnet coupling brake were pursued. This research shows that the LTA is a powerful and efficient tool to aid development and optimization of energy system devices like permanent magnet couplings.

4. FEM MODELING FOR THE PROTOTYPE OF A LINEAR RELUCTANCE MACHINE

4.1 Introduction

In the manufacturing industry, many production lines need conveyance systems to pick and transport small, thin and light components. The technologies normally applied, such as, robot arm and air conveyor, generally require complex control systems in order to avoid operating stability issues. For the transportation of small components containing ferromagnetic material, an electromagnetic device such as a linear machine has been investigated as a potential technology. The prototype of a specific linear reluctance machine was developed to investigate its capabilities. Of particular interests are the possibilities to ease mechanical complications, simplify the control system and reduce the “lost” component count of an existing air conveyor. A preliminary “demonstration – of – concept” prototype is shown in Fig.4.1 and is also described in Fig.4.2 of reference [16]. It consists of a series of

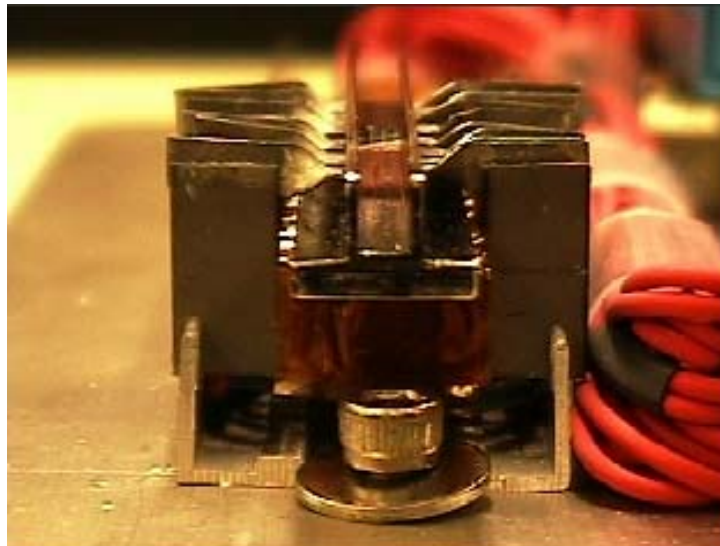


Fig.4.1 x – y plane view of prototype demo

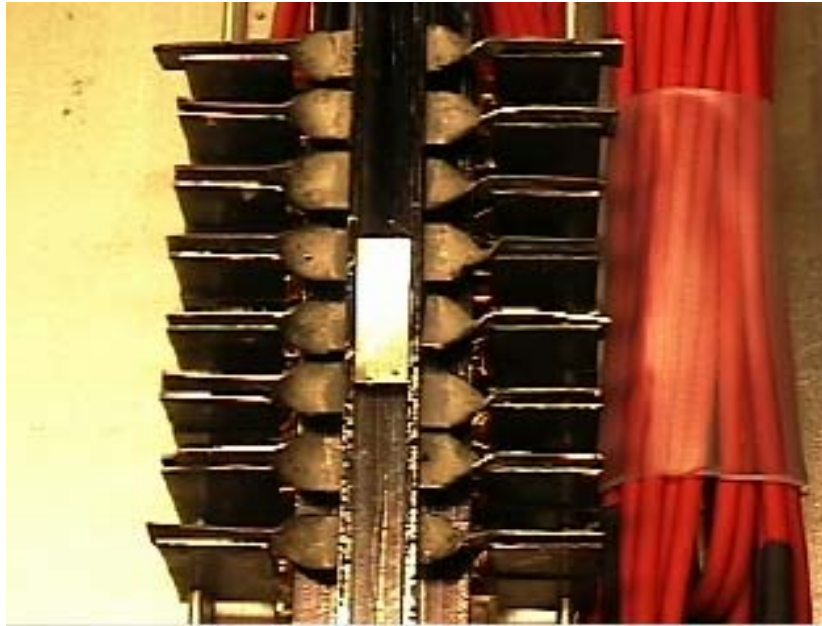


Fig.4.2 x – z plane view of prototype demo

Individual U type cores, which were constructed from transformer laminations, aligned in the x-y directions and stacked in the transporting direction (z-direction, normal to plane of photograph), and an aluminum channel set between the pole tips of the cores. The channel is applied to prevent the small components getting attached to the pole tips due to attractive forces in the x-direction, which can be greater than the transporting forces in the z-direction. The excitation coils were wound on the bottom part of the laminations. A PLC (Programmable Logic Controller) is used to adjust the transporting rate by controlling the sequential excitation of the coils from a power supply.

Although a functioning prototype had been demonstrated, due to the relative novelty of this type of linear reluctance machine, empirical methods alone are not sufficient and efficient to advance the development and investigate production oriented alternative configurations. Consequently, modeling and simulation techniques are needed to aid the design. For the discontinuous configuration of this

linear reluctance machine with very high leakage flux component, both the lumped-parameter circuit theory approach and the layer theory approach are difficult to apply and not accurate. In consequence, the finite element method was employed to model the prototype, investigate its performance, and inspect alternative topologies.

4.2 FE Modeling for the Linear Reluctance Machine Prototype

In order to shorten the time period as required for implementation in an industrial environment for the prototype development, we avoided the use of complicated and time consuming 3-D FE (Finite Element) modeling work and employed the 2-D FE model. This required models in both the x-y and x-z planes with calibration techniques to relate the two views to one another. As shown in Fig. 4.3, the x-y plane FE model of the linear reluctance machine depicts a core lamination with excitation coil and the thin small component suspending between the pole-tips. We use this model to calculate levitation forces in the y-direction and attractive forces in the x-direction.

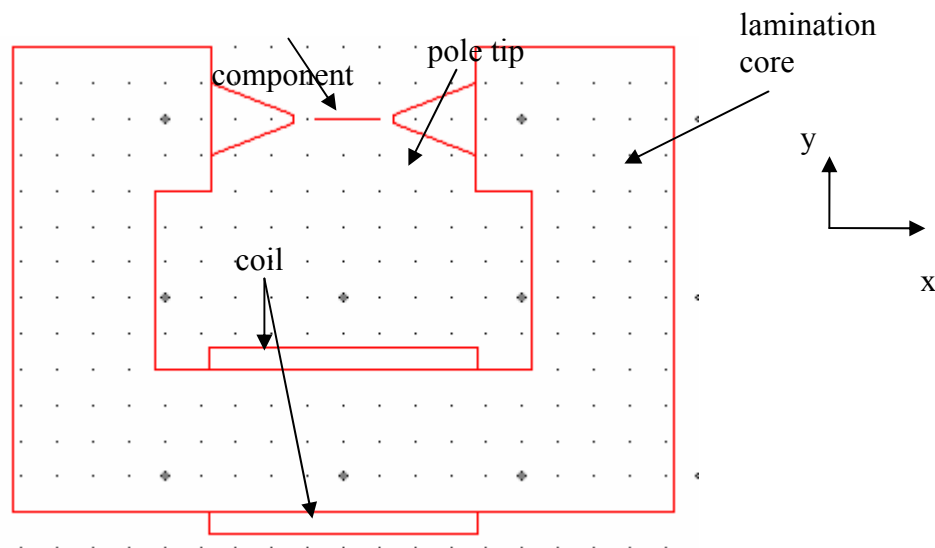


Fig. 4.3 x-y plane FE model

The assumptions for this x-y plane model are as follows:

- i) x-y plane FE model is assumed continuous in the z direction. All calculations are initially based on lengths of a meter.
- ii) DC currents of the excitation coils are in the z direction.
- iii) The tapering shape of poles represents the twisting of the laminations in the x-y direction. The permeability of the lamination is assumed to increase by a ratio which is width to thickness of the lamination at the very tip of the poles
- iv) The x-y plane model was calibrated to the prototype by matching calculated and tested minimum excitation ampere-turns which are needed to suspend the component. This can be calculated with some accuracy because the mass of the levitated component is known.

For the calculation of thrust forces in the z-direction, we use the x-z model of four pole pairs as shown in detail in Fig. 4.4a and Fig.4.4b. The assumptions for this x-z model are:

- i) Each lamination is modeled by cutting at the middle of the bottom edge, on the center line of the excitation coil, and extending the flap, thus formed, out in the x direction, as shown in Fig. 4.4a.
- ii) As shown in Fig. 4.4b, lamination lengths in the model join the outside edges of each half coil. These lengths have infinite permeability as this is a fictitious component to complete the magnetic circuit;
- iii) The representation of the pole – tip regions is completed by a decreasing permeability out to the surface of the airgaps.

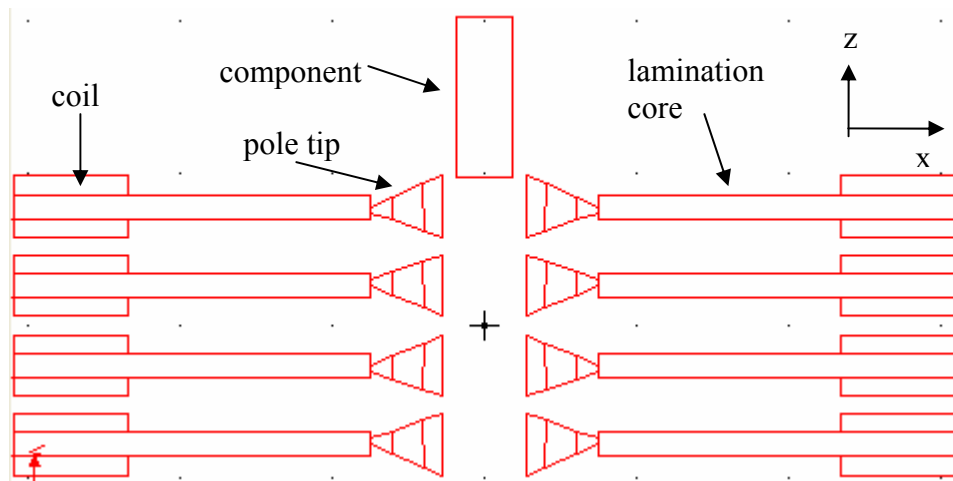


Fig. 4.4a x-z plane FE model for 4 extended out cores

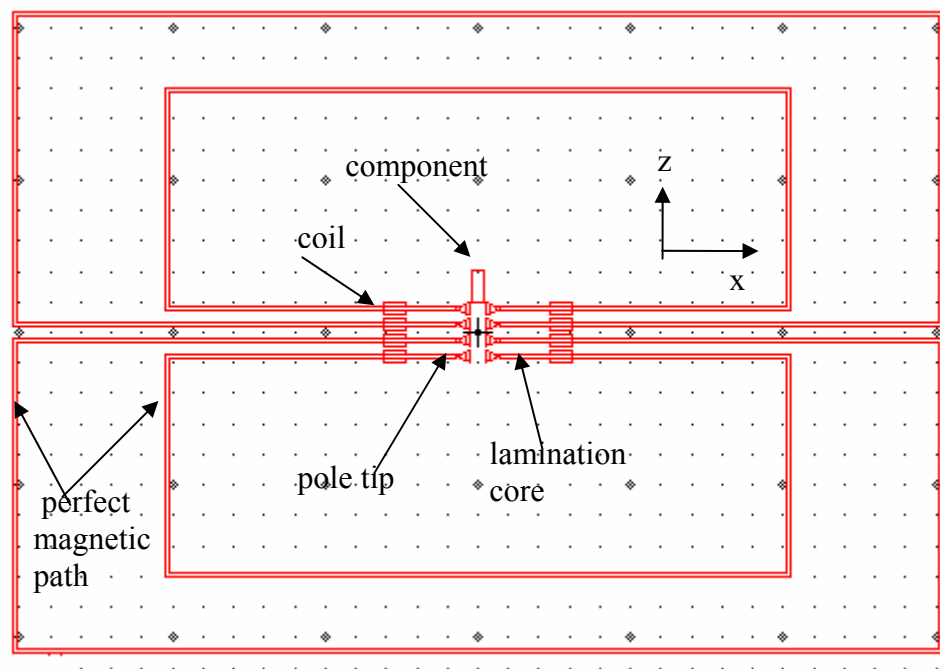


Fig. 4.4b x-z plane FE model for 4 extended out laminations with fictitious parts

- iv) Because the channel side-wall forces (x-direction) calculated in the x-z model must be equal to those calculated in the x-y model, a calibration coefficient is established for these two models.

To solve the two FE models of the linear reluctance machine, commercial FEA (Finite Element Analysis) software Maxwell 2D was employed.

4.3 FEA Software Maxwell 2D

Maxwell 2D is an interactive software package for analyzing electromagnetic and electromechanical problems using the 2-D finite element method. It is easy to use and can provide accurate simulation results. The simulator of Maxwell 2D can solve field equations for electrostatic, magnetostatic, eddy current and transient problems, etc.

Excitation coils of the linear reluctance machine are energized with DC currents that produce a static magnetic field. The magnetostatic field simulator is used for our case to solve the magnetic vector potential $A_z(x,y)$ in this field equation[17]:

$$J_z(x, y) = \nabla \times \left(\frac{1}{\mu_r \mu_0} (\nabla \times A_z(x, y)) \right) \quad (4.1)$$

where:

$A_z(x,y)$ is the z component of the magnetic vector potential.

$J_z(x,y)$ is the DC current density field flowing in the direction of transmission.

μ_r is the relative permeability of each material

μ_0 is the permeability of free space.

Given $J_z(x,y)$ as an excitation, the magnetostatic field simulator computes the magnetic vector potential $A_z(x,y)$ at all points in space. After $A_z(x,y)$ is computed, the magnetic flux density, B, and the magnetic field H in the x-y plane can then be computed using the relationship:

$$B = \nabla \times A \quad (4.2)$$

$$H = \frac{B}{\mu_r \mu_0} \quad (4.3)$$

With obtained field quantities B and H, the force on an object can be calculated using the principal of virtual work. The equation is given below:

$$F_{plate} = \frac{dW(s,i)}{ds} \Big|_{i=const} = \frac{\partial}{\partial s} \left[\int_V \left(\int_0^H B \bullet dH \right) dV \right] \quad (4.4)$$

Where,

W(s,i) is the magnetic coenergy of the system.

s is the displacement that shows the direction of the force on the object.

i is the constant excitation current.

The basic procedures to solve the FEM problem in Maxwell 2D software are shown in Fig. 4.5. The executive commands menu is shown in Fig. 4.6. The check mark represents that the command is completed.

Following the general procedures, we created and solved the FE 2-D model of the prototype of the linear reluctance machine. The simulation results are presented in detail in the next section.

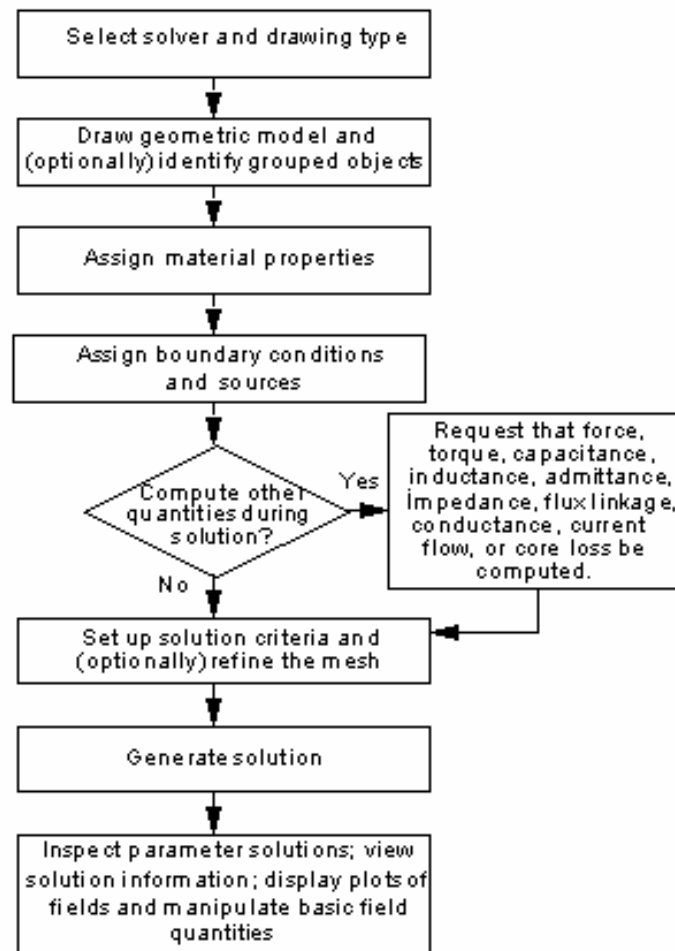


Fig. 4.5 General procedures of 2-D FEA in Maxwell 2D

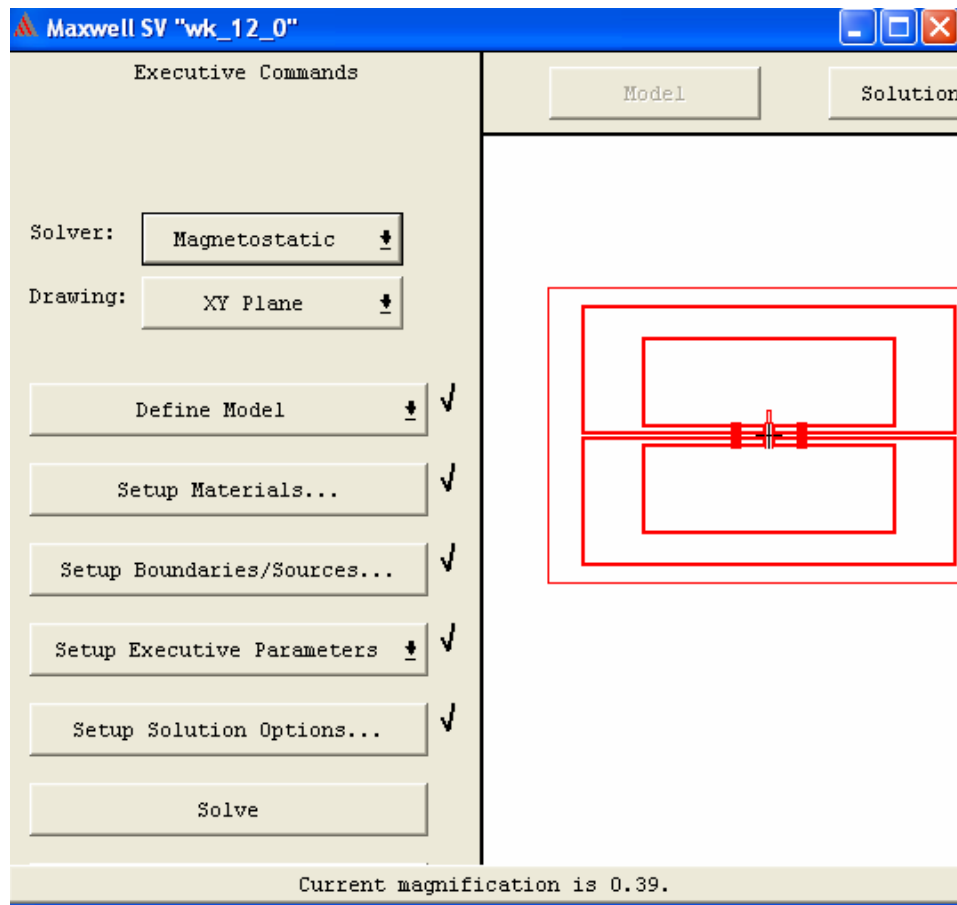


Fig. 4.6 User interface window of Maxwell 2D

4.4 Simulation Results for the Linear Reluctance Machine Prototype

For the x-y model of the linear reluctance machine, the magnetic flux distribution is shown in Fig. 4.7 which proves that the system has substantial flux leakage due to the thinness of the component, and the large airgap between the pole-pairs. The saturation condition of the lamination and component can also be inspected as in Fig. 4.8. In order to calibrate with the test results, the position of the part, where the levitation force balances with its weight, was found by a search process and determined through simulation. Subsequently all the levitation forces

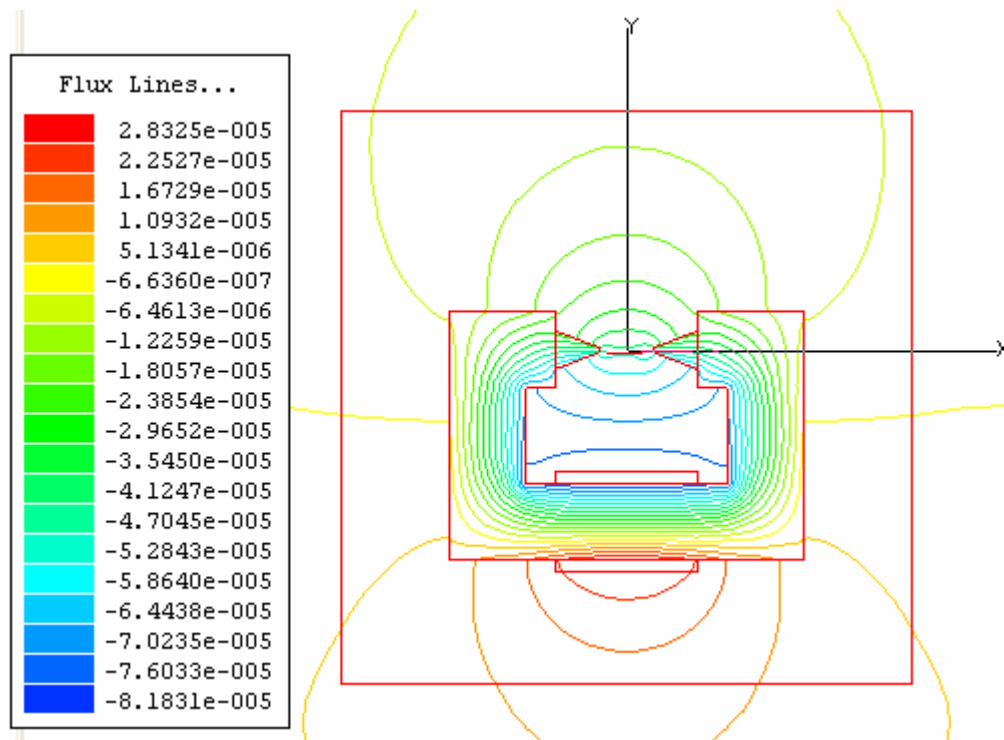


Fig. 4.7 Magnetic flux distribution for x-y plane model

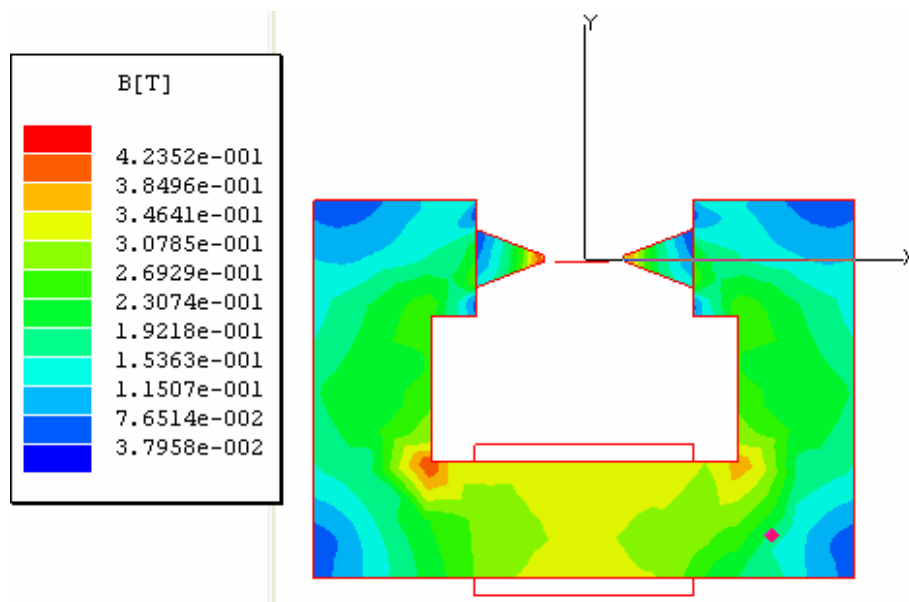


Fig. 4.8 Magnetic flux density distribution for x-y plane model

and channel side-wall forces were calculated based on this position. Also the minimum ampere-turns in the excitation coils that will suspend the component were obtained to calibrate with test results.

Another important characteristic of the linear reluctance machine is thrust force / component position in the channel in the z direction, which was calculated in the x-z model. Fig. 4.9 shows the case that the magnetic flux distribution when the component is about to enter the airgap of the first pole pair and the first two coils are energized. Fig. 4.10 and Fig. 4.11 show the change of the flux distribution when the component advances in the channel and the first two coils are still energized. The other cases when the component advances further in the channel and coils are energized sequentially are also analyzed. The actual simulation forces are determined and compared with test results for the prototype in the next section.

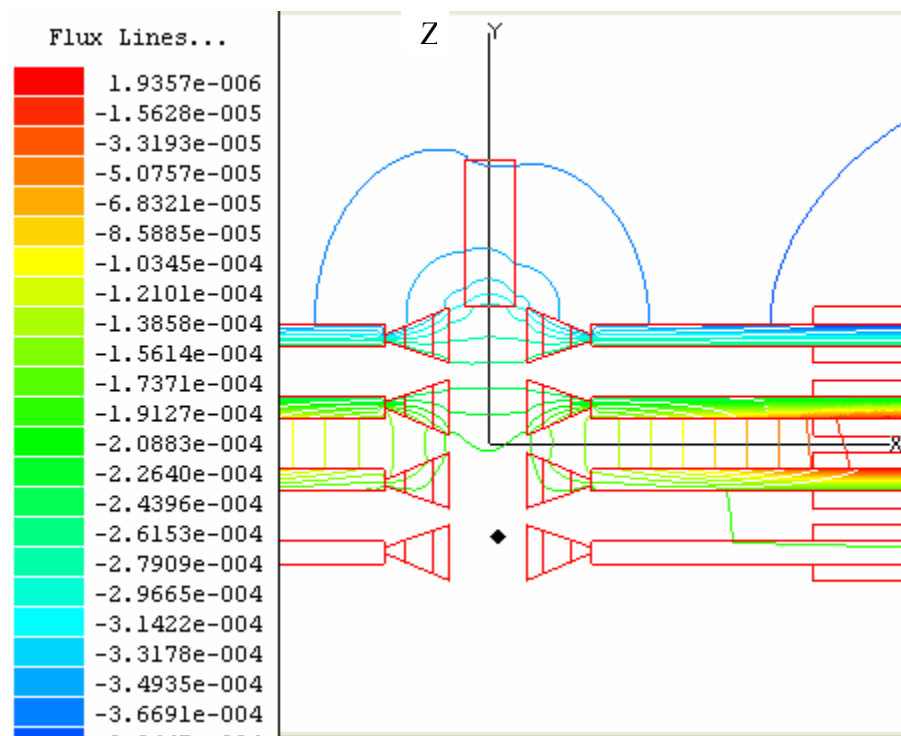


Fig. 4.9 Flux distribution of x-z model with the component at the starting point

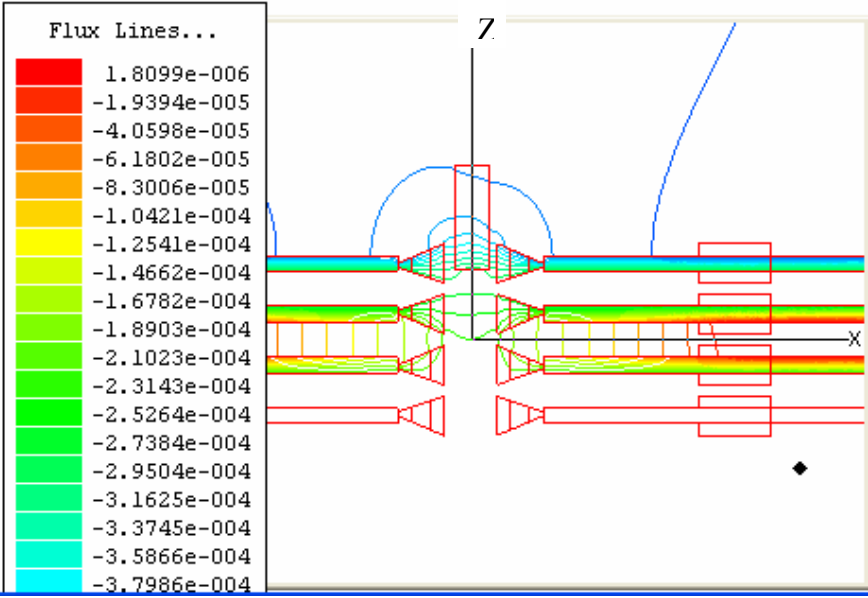


Fig. 4.10 Flux distribution of x-z model with the component between first pole pair

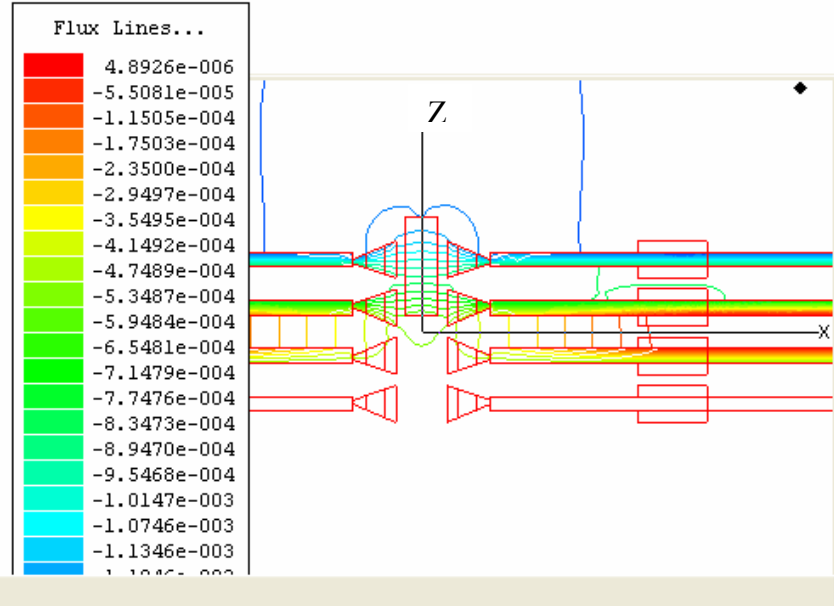


Fig. 4.11 Flux distribution of x-z model with the component between first and second pole pairs

4.5 Comparison of Simulation Results and Test Results

In order to establish the calibration coefficients, first it was required to locate the component position below the pole tip center line in the y direction for which maximum calculated levitation force was obtained. Next the ampere-turns were adjusted to match the calculated peak levitation force with the known weight of the component. Fig 4.12 shows the resulting curve obtained by a search process compared with the known weight of the component. In this figure, the position y was defined as 0 (mm) when the component is at the pole tip center line. Another calibration is between the x-y model and x-z model. Based on their common channel side-wall forces, the calibration coefficient was developed. After calibration, the simulation and test thrust forces as a function of ampere-turns for the case were as shown in Fig.4.9 and as compared in Fig. 4.13. The comparison shows good correlation.

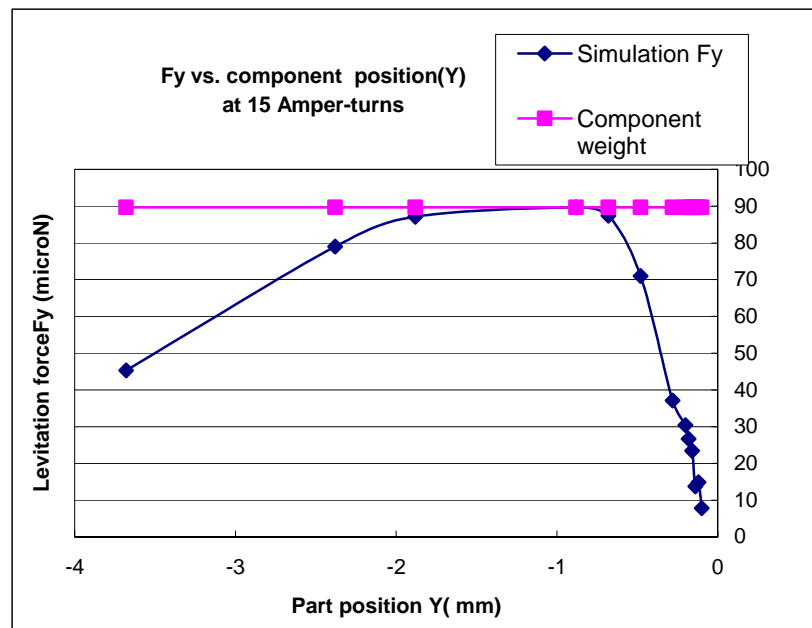


Fig. 4.12 Calibration based on levitation force in x-y model

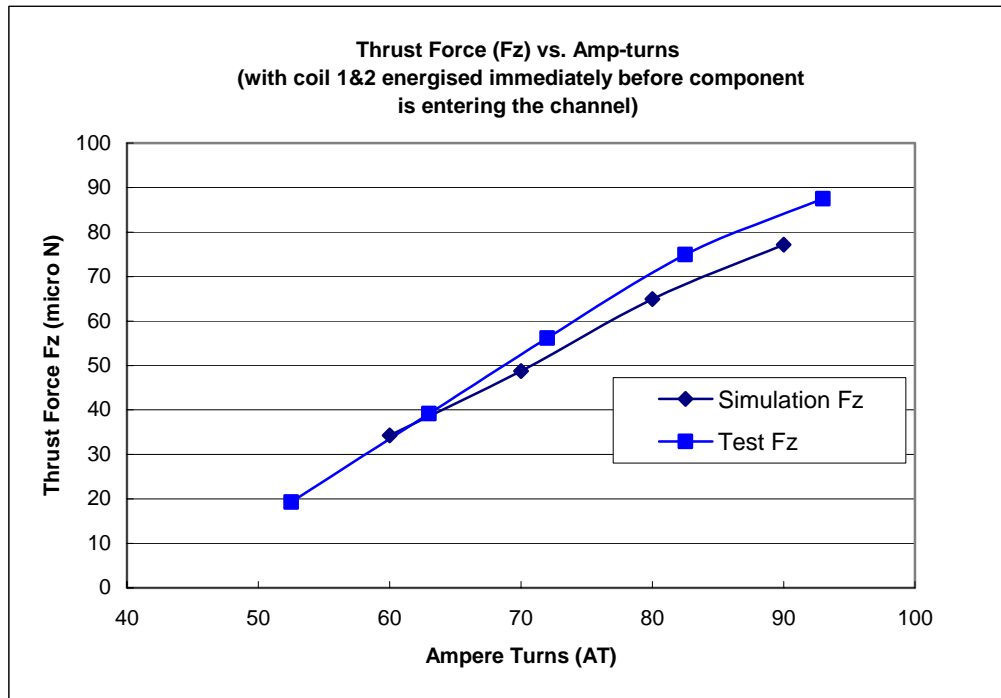


Fig. 4.13 Comparison of simulation and test thrust force / ampere-turn characteristics

The characteristic of force/component position calculated from x-z model compared with the average measured thrust force is shown in Fig. 4.14. In this figure, to facilitate understanding, it is noted that the position that the component is about to enter the channel is at position 0(mm). The absolute value of Z , $|z|$, increases as the component advances in the channel. The sequencing of coil energization can be optimized based on these characteristics.

The actual side-wall force F_x was determined by a test applying the indirect measure approach. The force was tested by inclining the prototype with a series of fixed currents and finding the angle of inclination at which the component is about to move. Under this condition the thrust force must be equal to the sum of the component weight at the angle of inclination plus the friction force between the component and the side-wall of the channel. The friction force is determined as the product of the coefficient of friction and the side-wall force.

Fig. 4.15 shows the characteristics of channel side-wall force F_x as a function of component position Z compared with the maximum measured channel side-wall force. These characteristics provide important information for choosing the channel material and adjusting the channel width in order to transport the small components successful and stably.

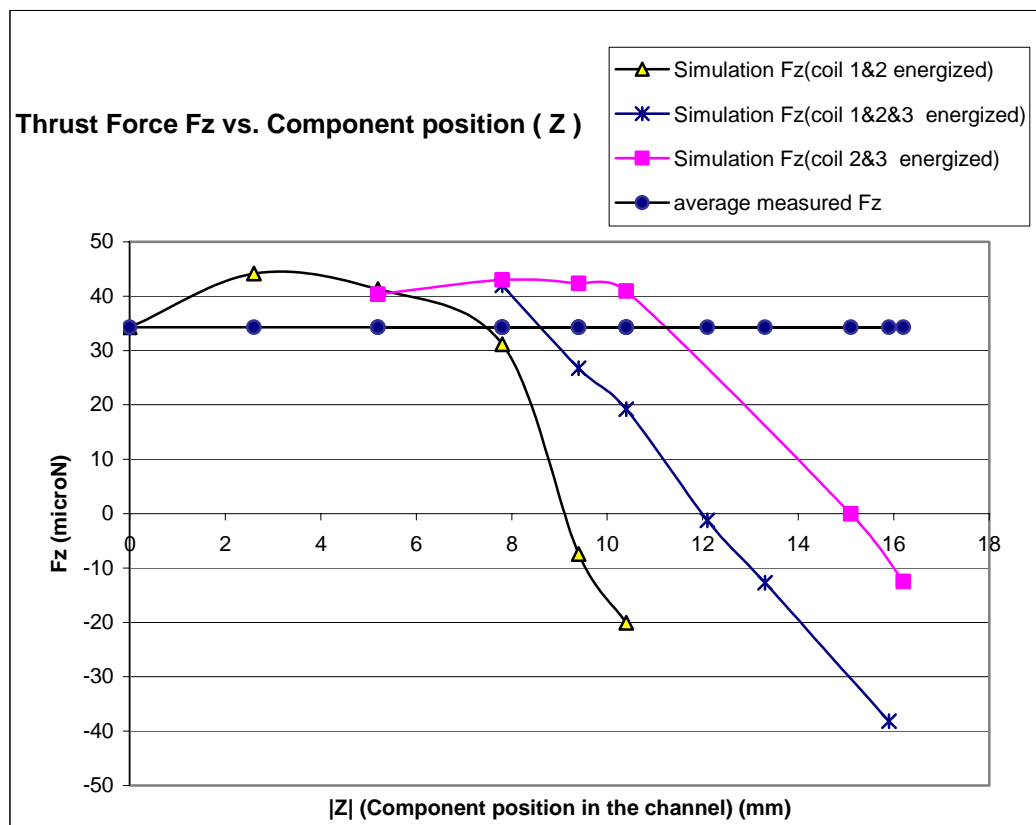


Fig. 4.14 Comparison of simulated and test characteristics of thrust force / component position (Z)

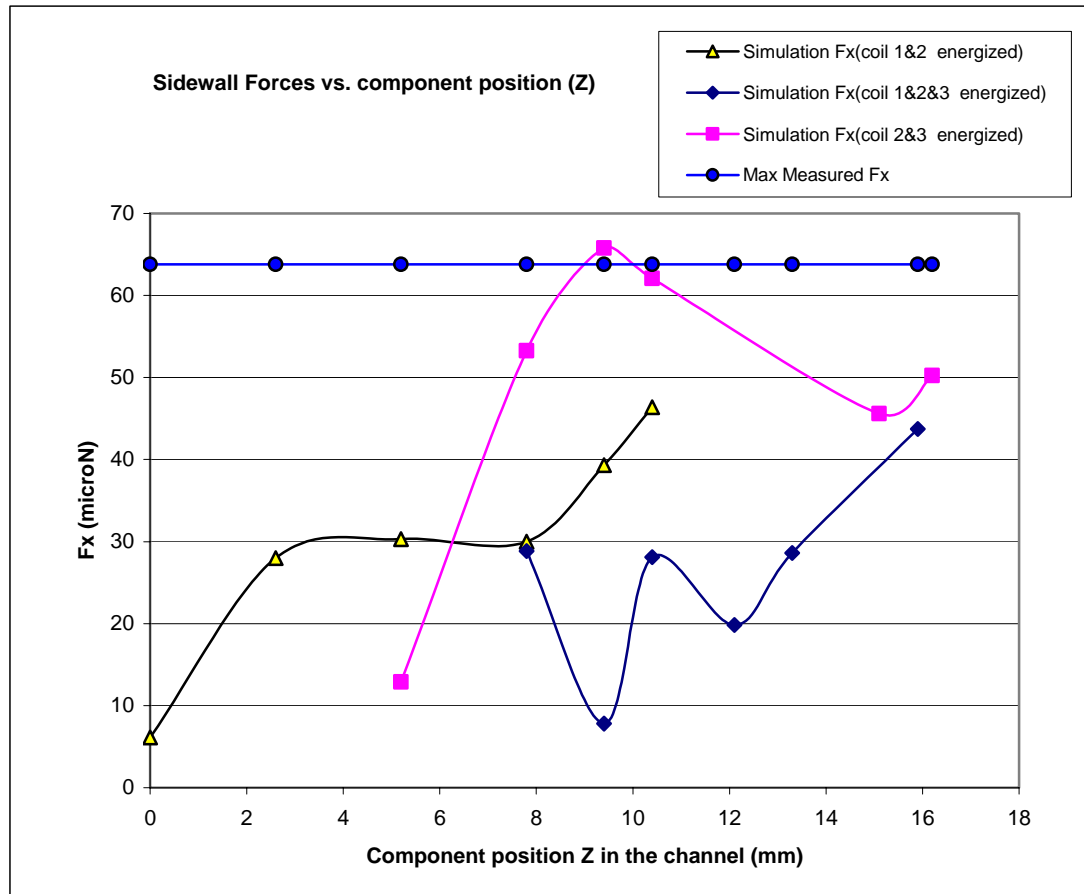


Fig. 4.15 Channel side-wall force/ component position (Z)

4.6 FE Modeling for the Production Machine

A conceptual design for the production machine was proposed based on the successful validation of the prototype machine. Although the topology of the production machine was substantially different (as shown in Fig. 4.16 and Fig. 4.17) from the prototype in order to meet the requirements of the final production system, such as adaptability to transport different sizes of components and limited space envelope, the modeling techniques used for the prototype are still valid. Following the similar procedures as used for the prototype modeling, the x-y plane FE model and the x-z plane FE model of the production machine are shown in

Fig.4.16 and Fig.4.18 respectively. There are two important improvements in the models due to the optimization design of the production machine. One is that the permeability of the poles was kept same over the entire region because all poles were made by cutting instead of twisting in the production machine. Another improvement is that coils were wound symmetrically near the pole-pairs instead of wound on the bottom of the laminations. This is effective for saving the vertical space in the production machine as well as placing the mmf (magnetomotive force) close to the airgap. Overall this configuration should be more effective, adjustable and manufacturable.



Fig. 4.16 x-y plane model of the production machine

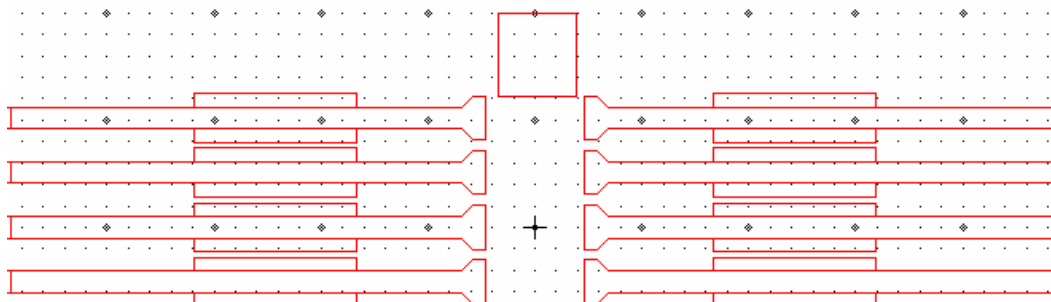


Fig. 4.17 x-z plane view of the production machine

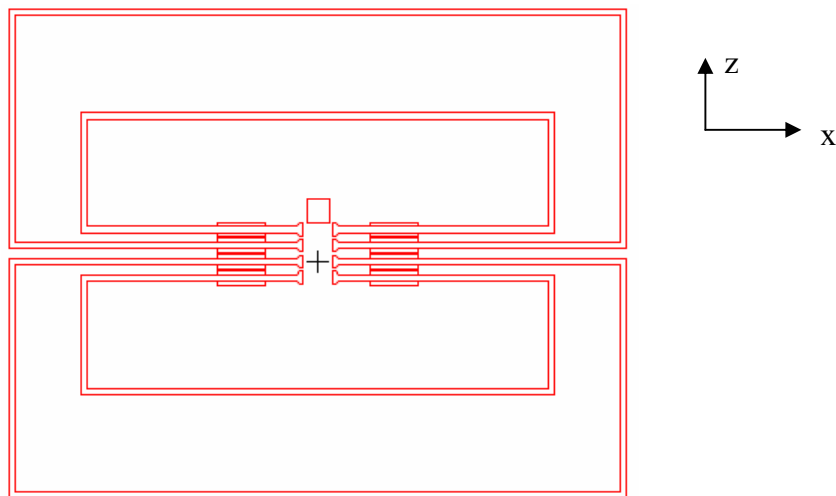


Fig. 4.18 x-z plane model of the production machine

Due to the short time period for this research project and relatively long time period required to make the production machine, the detailed simulation work was not required. Simulations using the models shown in Fig.4.16 and Fig.4.18 were used to investigate the viability of the proposed production machine to transport several different sizes of components. Fig. 4.19 to Fig. 4.21 show the preliminary performance prediction for the production machine with various size components for which the airgap of the machine could be adjusted. Typical dimensions (unit in mm) of the components for which the data is given in Fig.4.19 to 4.21 were: component 1 ($10.4 \times 3.6 \times 0.0235$); component 2 ($10.8 \times 2.9 \times 0.0235$); component 3 ($7.75 \times 7.23 \times 0.04995$). The ratio of thrust force to channel side-wall force is an important factor to investigate the performance of the linear reluctance machine while the friction coefficient of the channel is not negligible. For example, while the friction coefficient of the channel is around 1, it is required that the force ratio be kept larger than 1 through the channel in order to transport the components successfully. Without calibrating with experimental results, the FE models still can provide valuable information for the performance of the production machine using the force ratio.

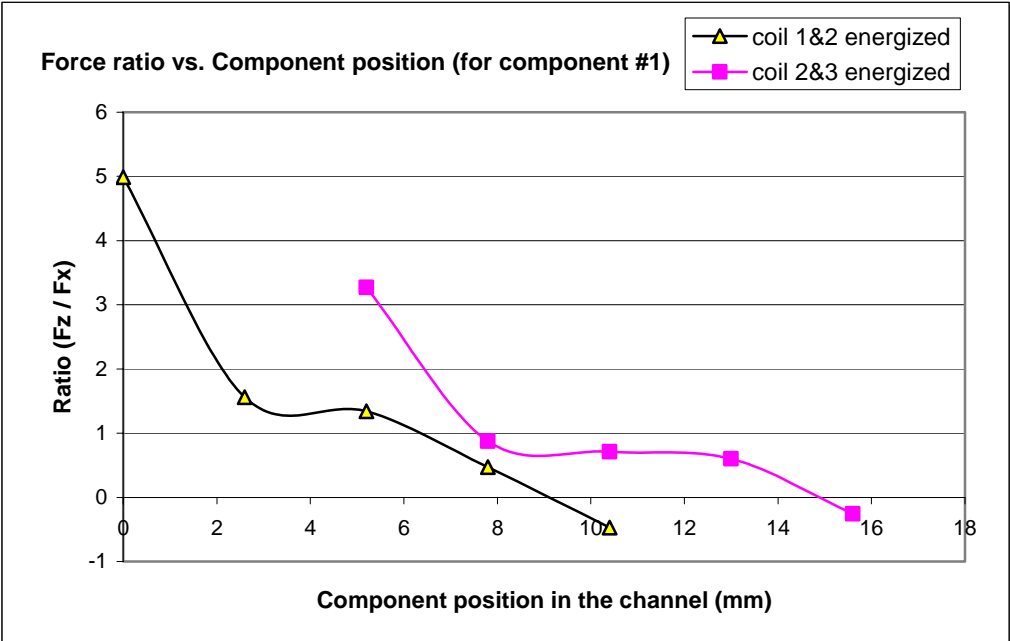


Fig. 4.19 Force ratio (F_z / F_x) for the production machine with component #1

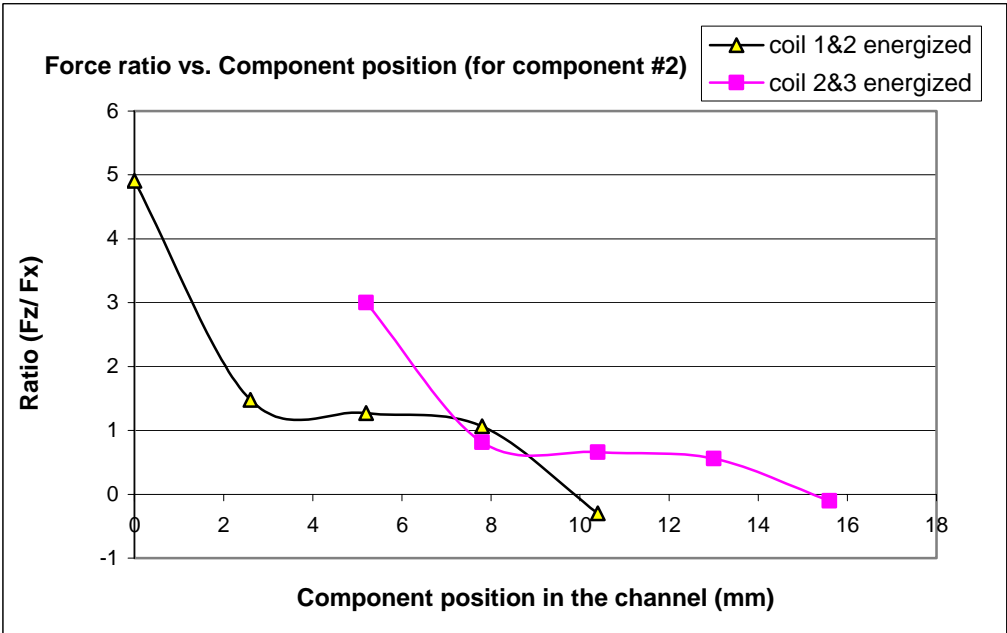


Fig. 4.20 Force ratio (F_z / F_x) for the production machine with component #2

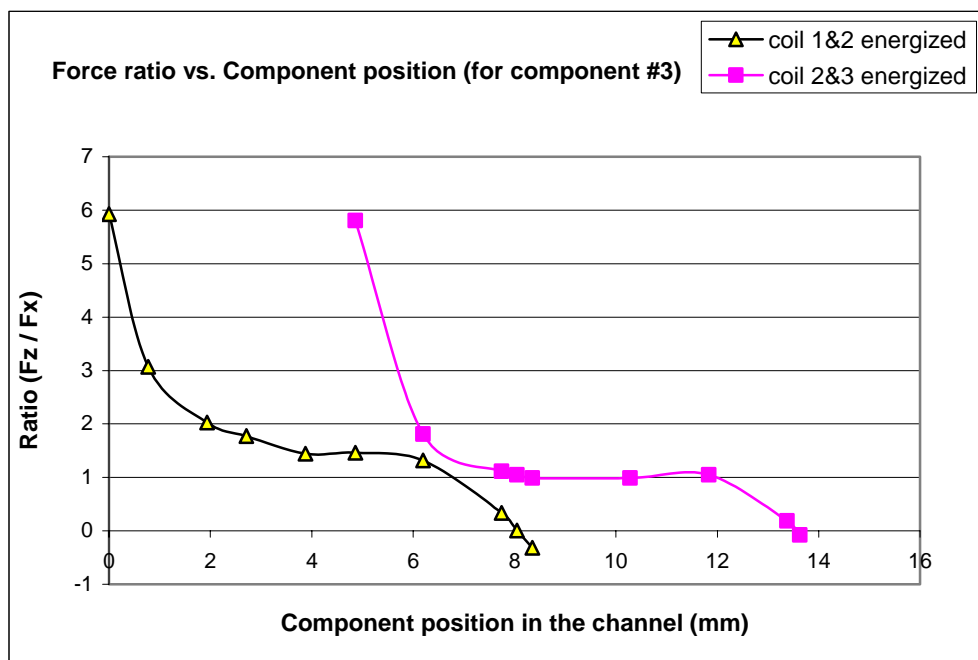


Fig. 4.21 Force ratio (F_z / F_x) for the production machine with component #3

4.7 Summary

The prototype of a linear reluctance machine is modeled with the 2-D FEM (Finite Element Method) and simulated with the Maxwell 2D magnetostatic simulator. Due to the complicated electromagnetic configuration of the prototype, two 2-D FE models (x-y model and x-z model) and special calibration techniques applying test results are adopted to consider the 3-D effects. The simulation work helped confirm the functionality and force characteristics of the prototype and provided further suggestions to optimize the prototype and refine new generation products. Also the FE model for the production machine was developed and preliminary performances predictions were accomplished. With more research time allowed, the more accurate model with 3-D FEM should be pursued to improve the simulation work.

5. CONCLUSIONS AND SUGGESTIONS FOR FUTURE WORK

5.1 Conclusions

This thesis work employed respectively two EMA (Electromagnetic Analysis) methods, LTA (Layer Theory Approach) and FEM (Finite Element Method), to analyze two types of new energy system devices, the permanent magnet coupling and the prototype of a linear reluctance machine. LTA is a suitable and efficient tool for devices like linear induction machines and permanent magnet couplings, which include sheet conductor as secondaries. Finite element analysis of such systems has been employed but has numerous disadvantages including large memory requirements and very slow computational times. The layer theory approach benefits from its basic simplicity and the strength of the applicable analytical techniques of multiple harmonics and the Russell – Norsworthy functions. 2-D FEM (Finite Element Method) is more appropriate to simulate the prototype of the novel linear reluctance machine in order to obtain sufficient accuracy in a relatively restricted development time period.

The two modeling works successfully accomplished the objective to aid the development and optimization design of these two new energy system devices in a short time period. For permanent magnet couplings, the LTA program can predict the characteristics of torque/slip speed and axial force / slip speed and they have good correlations with test results. The program also is a useful tool for the parametric design study of the permanent magnet coupling. It requires short computing time and low computing memory, and easy to set up. It is anticipated that the US Navy's testing requirements for a large "silent" braking system can be designed using LTA techniques. 2-D FEM in cooperation with the calibration technique can model the complicated 3-D configuration of the prototype of the linear reluctance machine with satisfying accuracy and short simulation time. In the 2-D models, flux distribution, leakage flux and flux density can be visually investigated. Characteristics of levitation force, channel side-wall force and thrust

force vs. component position are able to be simulated. The developed results show that it is a very valid approach during the prototype concept-proof and demonstration phase of the linear reluctance machine.

The research work of this thesis proves that LTA and FEM are powerful and efficient EMA (Electromagnetic Analysis) tools for development of energy system devices.

5.2 Suggestions for Future Work

For the LTA program, recommendations for future work are below:

- 1) Develop a more accurate model for effects of temperature.
- 2) Take into account the end effects of permanent magnetic couplings in the model.
- 3) Make the model applicable to dynamic studies and more derivative devices.

For the electromagnetic model of the prototype of the linear reluctance machine, suggestions for future work are as follows:

- 1) Improve the 2-D FE model technique to simulate the device without calibration procedures.
- 2) Apply 3-D FEM to model the linear reluctance machine more accurately.

BIBLIOGRAPHY

1. Stephen J.Chapman, *Electric machinery and power system fundamentals*, Boston, McGraw-Hill, c2002.
2. Peter Campbell, *Permanent magnet materials and their application* Cambridge University Press, September 1994.
3. Rexnord Corporation, *The future of power transmission is here! - Rex magnelink coupling*, 1997.
4. Korada Umashankar, *Introduction to engineering electromagnetic fields*, Singapore : Teaneck, N.J. : World Scientific, 1989.
5. Jianming Jin, *The finite element method in electromagnetics*, John Wiley & Sons, Inc,2002.
6. Simon Ramo, John R. Whinnery, Theodore Van Duzer, *Fields and waves in communication electronics*, John Wiley & Sons, Inc,1994.
7. C.A. Skalski, "Application of a general analysis for single-sided linear induction motors", *IEE conference on linear electric machine*, London, England, Oct. 1974.
8. K. Idir, G.E. Dawson, A.R. Eastham, "Modeling and performance of linear induction motor with saturable primary", *IEEE trans. on Industrial applications*, vol. 29, no.6, Nov. 1993.
9. J.P. Webb, *Application of the finite element method to electromagnetic and electrical topics*, Rep. Prog. Phys. 58, UK, 1995 .
10. Matthew N.O. Sadiku, *Numerical techniques in electromagnetics*, CRC press LLC, 2001.
11. Y.K. Cheung, S.H. LO, A.Y.T. Leung, *Finite element implementation*, Blackwell science Ltd, 1996.
12. A.C. Smith, Amged El-Wakeel, A. Wallace, "Formal Design optimization of PM drive couplings", *IEEE 37th Industry Applications Conference*, vol.1. Page(s): 205 -211, Oct. 2002.
13. Kenneth J. Anderson, Ron Woodard, Alan Wallace, "Test and demonstration results of a new magnetically coupled adjustable speed drive", *Proc. IECEC'01*, Georgia, July/August 2001.

14. A.C. Smith, S. Williamson, A. Benhanma, etc., "Magnet Drive Couplings", *IEE Ninth International Conference on Electrical Machines and Drives*, 1999.
15. Nobuo Fujii, Masashi Fujitake, "Two-dimensional drive characteristics by circular-shaped motor", *IEEE trans. on Industry applications*, vol. 35, no. 4, July/August, 1999.
16. A. Wallace, K. Rhinefrank, Y. Li, "Development of a linear reluctance machine for transport of small components", submitted to IAS conference 2004.
17. Ansoft corp. *Maxwell 2D help documents*, February 2002.